Geological Society of America
3300 Penrose Place
P.O. Box 9140
Boulder, CO 80301
(303) 447-2020 • fax 303-357-1073
www.geosociety.org

Geological Society of America
Special Paper 403
2006

Diachronous histories for the Dabie-Sulu orogen from high-temperature geochronology

M.L. Leech*
Geological and Environmental Sciences, Stanford University, Stanford, California 94305, USA
L.E. Webb
Department of Earth Sciences, Syracuse University, Syracuse, New York 13244, USA
T.N. Yang
Institute of Geology, Chinese Academy of Geological Sciences, Beijing, 100037, China

ABSTRACT

New U-Pb sensitive high-resolution ion microprobe (SHRIMP) dating of zircon from the ultrahigh-pressure Sulu terrane, eastern China, records three events in the evolution of the orogen. Peak ultrahigh-pressure and retrograde metamorphism in the Middle to Late Triassic (ca. 230–200 Ma) is recorded in zircon mantles and rims; cathodoluminescence imaging, grain morphology, and U-Th-Pb and rare earth element chemistry cannot distinguish between ultrahigh-pressure and retrograde zircon growth. Comparison of high-temperature thermochronology for the Sulu and Dabie–Hong'an areas suggests that peak ultrahigh-pressure metamorphism in Sulu took place at ca. 230 Ma, postdating Dabie–Hong'an by 10 m.y.; this age disparity has implications for collision-subduction-exhumation models for the entire Qinling–Hong'an–Dabie–Sulu orogen and suggests that Sulu was a separate ultrahigh-pressure slab that was never adjacent to Dabie. Relict zircon cores and mantles preserve protolith ages between 700 and 790 Ma, reflecting the Yangtze craton affinity of the Sulu terrane and supporting other evidence indicating that the suture between the Yangtze and Sino-Korean cratons lies along the Yantai-Qingdao-Wulian fault zone. Late Jurassic to Early Cretaceous ages from a pegmatite vein near the suture probably reflect early melting related to a widespread magmatic event that affected the northern margin of the Dabie-Sulu belt.

Keywords: U-Pb zircon SHRIMP dating, Qinling–Hong'an–Dabie–Sulu orogen, eastern China, Triassic ultrahigh-pressure (UHP) metamorphism, Yangtze craton.

*Present address: Department of Geosciences, San Francisco State University, San Francisco, California 94132, USA.

Leech, M.L., Webb, L.E., and Yang, T.N., 2006, Diachronous histories for the Dabie-Sulu orogen from high-temperature geochronology, *in* Hacker, B.R., McClelland, W.C., and Liou, J.G., eds., Ultrahigh-pressure metamorphism: Deep continental subduction: Geological Society of America Special Paper 403, p. 1–22, doi: 10.1130/2006.2403(01).

INTRODUCTION TO THE QINLING–HONG'AN–DABIE–SULU OROGEN

The Sulu terrane (Fig. 1), the eastern extension of the larger Qinling–Hong'an–Dabie–Sulu orogen, was the one of the first ultrahigh-pressure (UHP) subduction zone complexes shown to contain microdiamond, requiring UHP metamorphism at pressures in excess of 3.2 GPa at >130 km depth (Sobolev and Shatsky, 1990; Xu et al., 1992). Ultrahigh-pressure metamorphism occurred during the Triassic northward subduction of the Yangtze craton beneath the Sino-Korean craton (e.g., Liou et al., 1996; Hacker et al., 2000, 2004; Chen et al., 2003). Mineralogical evidence for Early to Middle Triassic UHP metamorphism is found in minor eclogite and garnet peridotites, and their host quartzofeldspathic gneisses, that all followed the same pressure-temperature-time (*P-T-t*) path during subduction

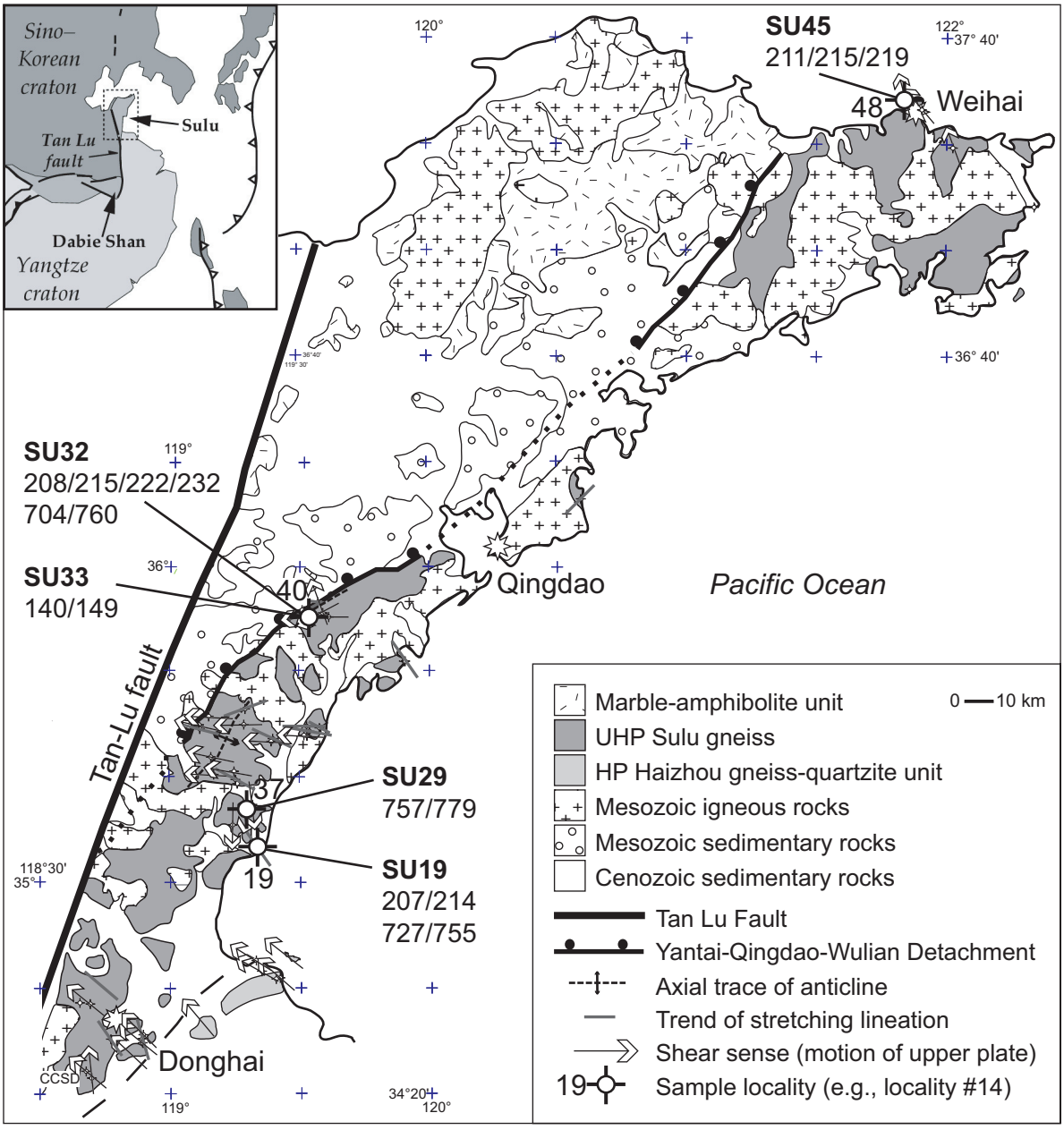

Figure 1. General geologic map of the Sulu terrane, part of the Shandong Peninsula, eastern China (after Wallis et al., 1999; Webb et al., this volume). Sample numbers for U-Pb sensitive high-resolution ion microprobe (SHRIMP) dating are shown in bold (Appendix 1 contains complete U-Th-Pb data). Weighted mean ages (in Ma) summarize age data for each sample. The Qinling–Hong'an–Dabie blocks are shown on the inset map in medium gray (Dabie is labeled, the Qinling and Hong'an blocks are further west). UHP—ultrahigh pressure.

and exhumation (e.g., Xu et al., 1992; Liou et al., 1996, and references therein; Tabata et al., 1998). Conditions for UHP metamorphism in the Dabie and Sulu areas were ~600–800 °C and from to 3.0–4.0 GPa (W.G. Ernst, 2005, personal commun.). Exhumation of these UHP rocks to middle- to upper-crustal levels was complete by the latest Triassic to Early Jurassic (e.g., Hacker et al., 2000; Ratschbacher et al., 2000; Webb et al., 1999, this volume), and likely proceeded during coeval detachment faulting/shearing and gneiss dome formation (Webb et al., 2002, this volume; Leech et al., 2003). The northern part of the orogen experienced extensive magmatism in the Early Cretaceous (Hacker et al., 1998; Ratschbacher et al., 2000; Grimmer et al., 2002) and later oblique sinistral offset along the Tan-Lu fault (Fig. 1).

An extensive collection of $^{40}Ar/^{39}Ar$ ages for the Hong'an, Dabie, and Sulu areas (e.g., Hacker et al., 2000, and references therein; Webb et al., 1999) documents synexhumation cooling of the UHP rocks to the middle to upper crust, but the precise timing of UHP metamorphism across the orogen remains elusive. Various workers have used high-temperature thermochronometry (U-Th-Pb, Sm-Nd, and Rb-Sr) to address this issue, but many individual attempts are plagued by large analytical errors, a lack of sufficient data, age ranges spanning both peak and retrograde metamorphism, and assumptions about the ~2000 km orogen having a uniform subduction-exhumation history. Here we present new U-Pb SHRIMP (sensitive high resolution ion microprobe) dating of zircon for the Sulu terrane, compare this new data to the existing body of dating for the UHP metamorphic event, and discuss the implications for an orogenic model with UHP metamorphism taking place in the Sulu area ~10 m.y. after UHP metamorphism in the Dabie–Hong'an area.

NEW U-Pb SHRIMP DATING FOR SULU

Samples of UHP quartzofeldspathic gneiss (host rocks to eclogite) from three different areas in the Sulu terrane, and a mylonitized gneiss and pegmatite vein from near the Yantai-Qingdao-Wulian fault were collected to establish the timing of UHP metamorphism, retrograde metamorphism and exhumation-related deformation, and later magmatism, respectively. Quartzofeldspathic lithologies were chosen for the relative abundance of zircon that could be extracted for U-Pb SHRIMP dating; zircon can record a long history of growth recorded in relict internal parts of zircon grains, can record higher-temperature events (~1000 °C) than other thermochronometers (Cherniak and Watson, 2003), making dating peak metamorphic conditions more likely, and can record lower-temperature events during recrystallization. Three of these samples (SU29, SU33, and SU45) are the same samples from which other mineral phases were extracted for dating by the $^{40}Ar/^{39}Ar$ method in Webb et al. (this volume), the results of which are summarized in the following section.

Sample Preparation and Analytical Technique

A total of 143 zircon U-Pb SHRIMP analyses were completed for five samples (Fig. 2; see Appendix 1 for U-Th-Pb data for all analyses). Zircons were separated and mounted using standard sample-preparation methods for ion microprobe analysis (Williams, 1998), and U-Pb SHRIMP analyses, data reduction using *Squid*, and plotting using *Isoplot* followed standard techniques (Williams, 1998; Ludwig, 1999, 2001). No morphologic or color differentiation was made during handpicking for the sample mount. Separated zircons include euhedral, subrounded, and irregularly shaped grains that display clear core-mantle-rim zoning relationships under cathodoluminescence (CL) imaging (Fig. 3). SHRIMP analyses targeted rims that appeared to be metamorphic based on CL imaging (i.e., lack of zoning, rounded grain morphology); analysis of zircon mantles and cores was done for age comparison with metamorphic rims and to establish different growth domains within the zircons. Pb/U ratios were calibrated with reference standard R33 (419 Ma; Black et al., 2004), which was analyzed after about every fourth unknown analysis. Zircons were analyzed using the SHRIMP-RG (reverse geometry) at the Stanford–U.S. Geological Survey Microanalysis Center. U-Th-Pb data for each ~30 μm spot were collected in five scans.

Descriptions of Dated Samples

All five samples dated in this study came from the UHP Sulu gneiss unit (Fig. 1). Figure 2 shows Tera-Wasserburg concordia diagrams for all analyses from all five samples; these concordia plots include some discordant data and display mixing trends and discordance due to common Pb (all concordia plots [Figs. 2, 4, and 5] show data uncorrected for common Pb). All ages (single-grain or weighted mean ages [95% confidence level]) described for dating in this study are ^{207}Pb-corrected $^{206}Pb/^{238}U$ ages from concordant data or data within 1%–2% of concordance (see ages listed with concordia plots in Figs. 4 and 5); high U, high common Pb, and discordant analyses were excluded from age calculations.

Sample SU19

Sample SU19 is a quartzofeldspathic gneiss from the central part of the UHP Sulu terrane within the core of the large gneiss dome structure (locality 19: 35°10′N, 119°14′E; Fig. 1). Relict Proterozoic zircon domains in sample SU19 yield ages between 702 and 767 Ma; two distinct populations within that range give weighted mean ages of 727 ± 15 Ma (3 grains) and 755 ± 12 Ma (5 grains) from concordant analyses. These Proterozoic domains are generally bright cores and mantles with oscillatory zoning in cathodoluminescence (CL) imaging and have relatively high Th/U ratios between 0.6 and 1.7 (Figs. 2A, 3, and 4). Concordant Late Triassic analyses yield weighted mean ages for two age groups at 207 ± 3 Ma (5 grains) and 214 ± 4 Ma (4 grains); these ages result from uniformly nonluminescent, rounded metamorphic rims and have very low Th/U ratios (<<0.1) (Figs. 5 and 6; Appendix 1).

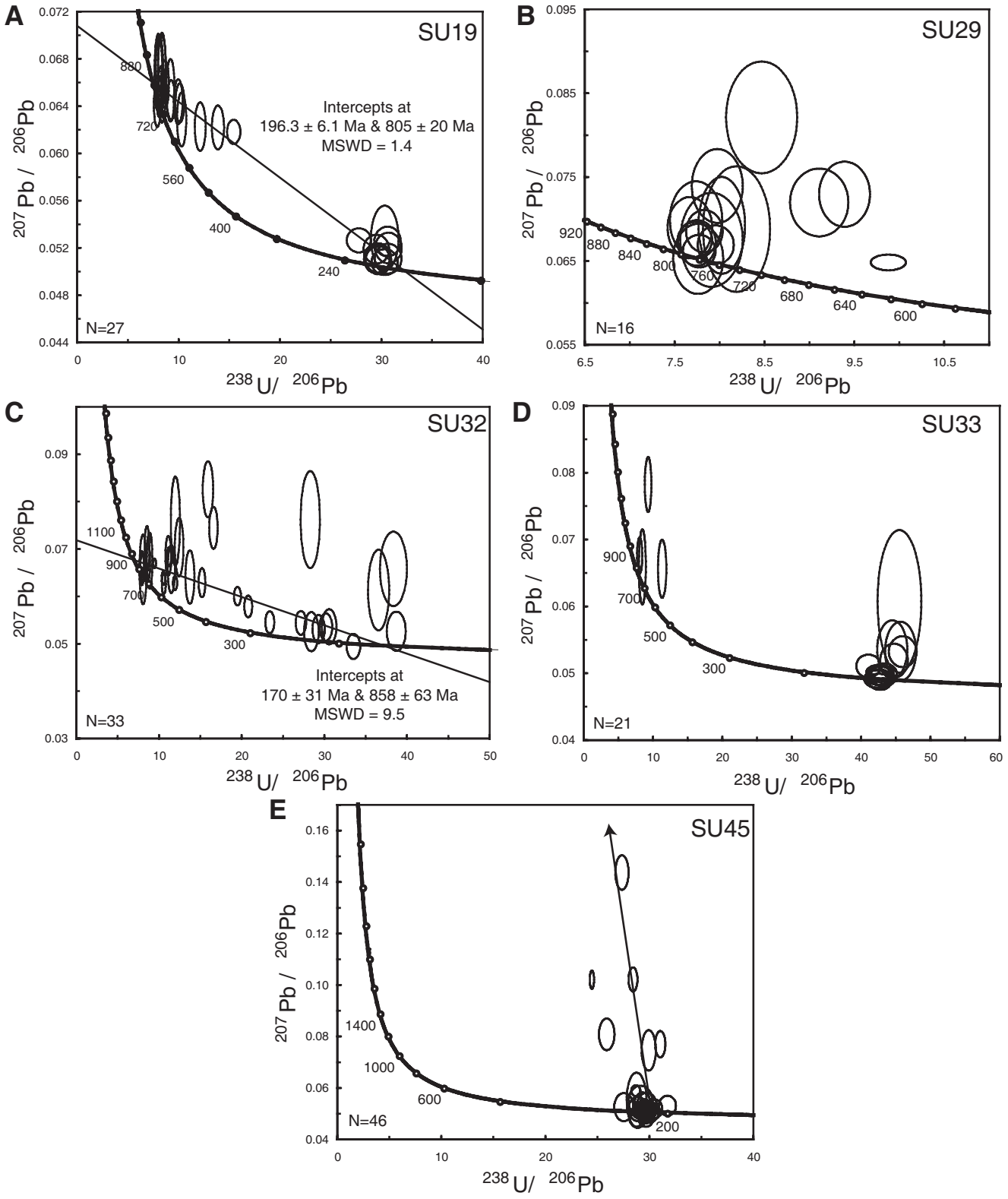

Figure 2. Tera-Wasserburg concordia diagrams for all zircon analyses from all samples (data uncorrected for common Pb; error ellipses are 2σ). A and C include intercept lines that show mixing for discordant data between Proterozoic and Mesozoic analyses for samples SU19 and SU32 (intercept ages are not used for interpretation—see weighted mean ages in Figs. 4 and 5). E shows a projection to common Pb ratio ($^{207}Pb/^{206}Pb$ = 0.86 based on Cumming and Richards, 1975) for six discordant analyses from sample SU45. *N* is the number of zircons analyzed for each sample. MSWD—mean square of weighted deviates.

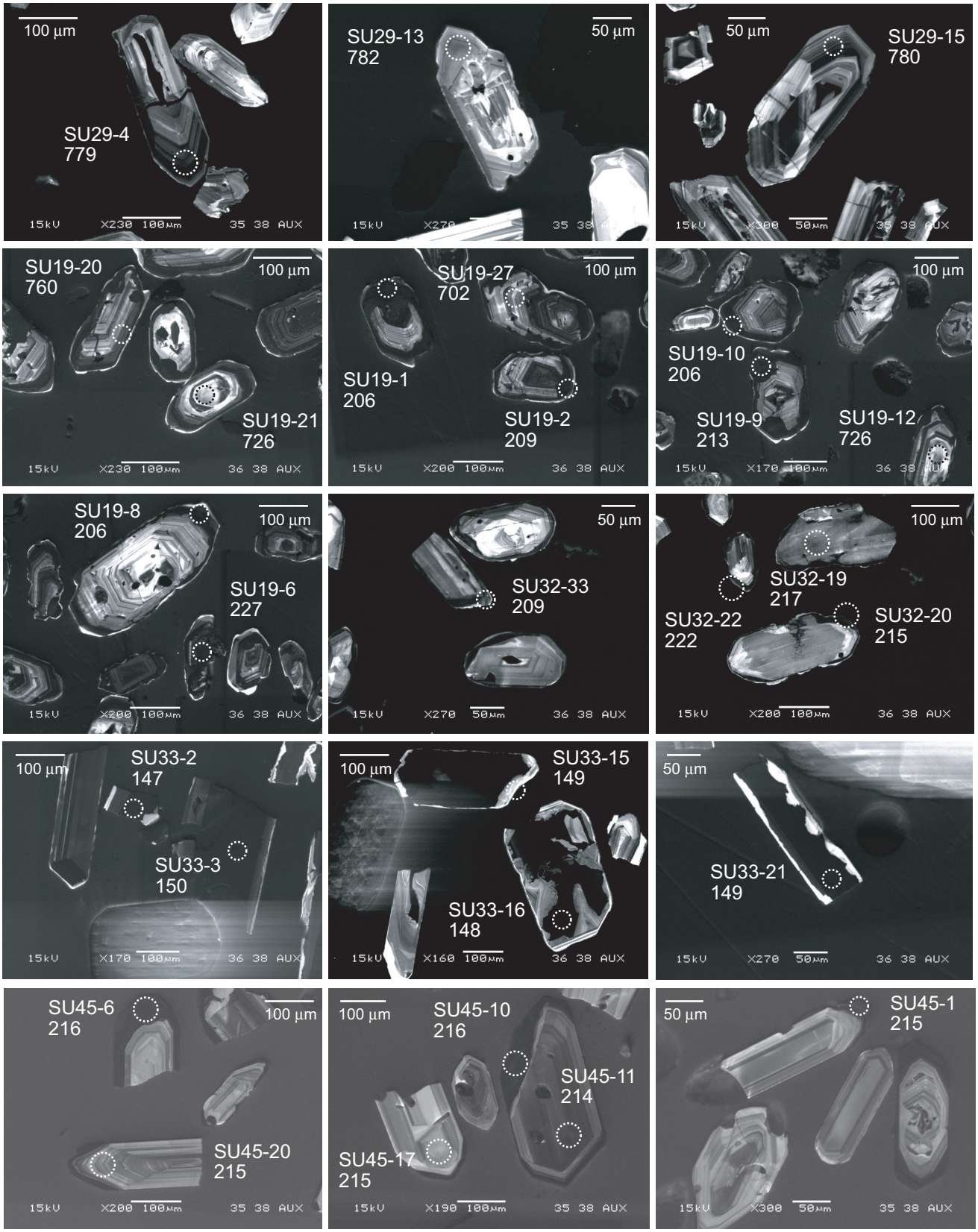

Figure 3. Cathodoluminescence (CL) images of representative analyzed zircons from each sample. Analysis number with corrected $^{206}Pb/^{238}U$ age and spot locations (dashed circles) correspond to those listed in Appendix 1. Streaking is due to charging on nonzircon grains.

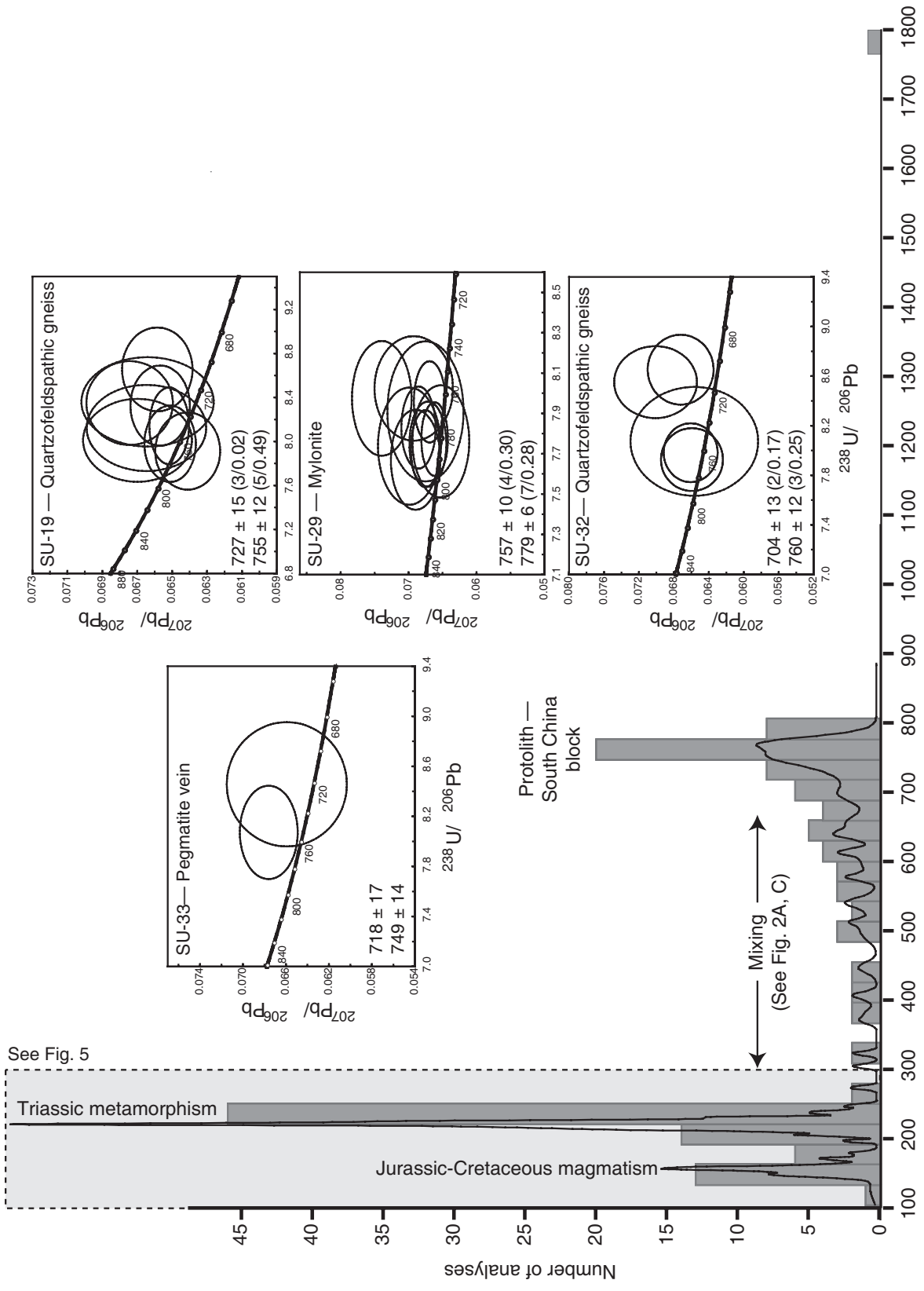

Figure 4. Histogram and probability density curve for all $^{238}U/^{206}Pb$ ages (^{207}Pb corrected) from all samples. Three main events are recorded: relict protolith ages from zircon cores (ca. 780–700 Ma), Triassic metamorphism (220–210 Ma), and Late Jurassic–Early Cretaceous magmatism (150–140 Ma); data between 700 Ma and 300 Ma represent mixing in samples SU19 and SU32. Tera-Wasserburg concordia diagrams show concordant and near-concordant Proterozoic analyses for samples SU19, SU29, SU32, and SU33 (data uncorrected for common Pb; error ellipses are 2σ); single-grain ages and weighted mean ages for multiple age groups in each sample are listed, with the number of analyses and mean square of weighted deviates (MSWD) included for those averages (in parentheses). Age groups delineated by weighted mean ages were determined based on weighted mean age plots of concordant data (data weighted by 2σ data-point errors; analyses high in common Pb were excluded).

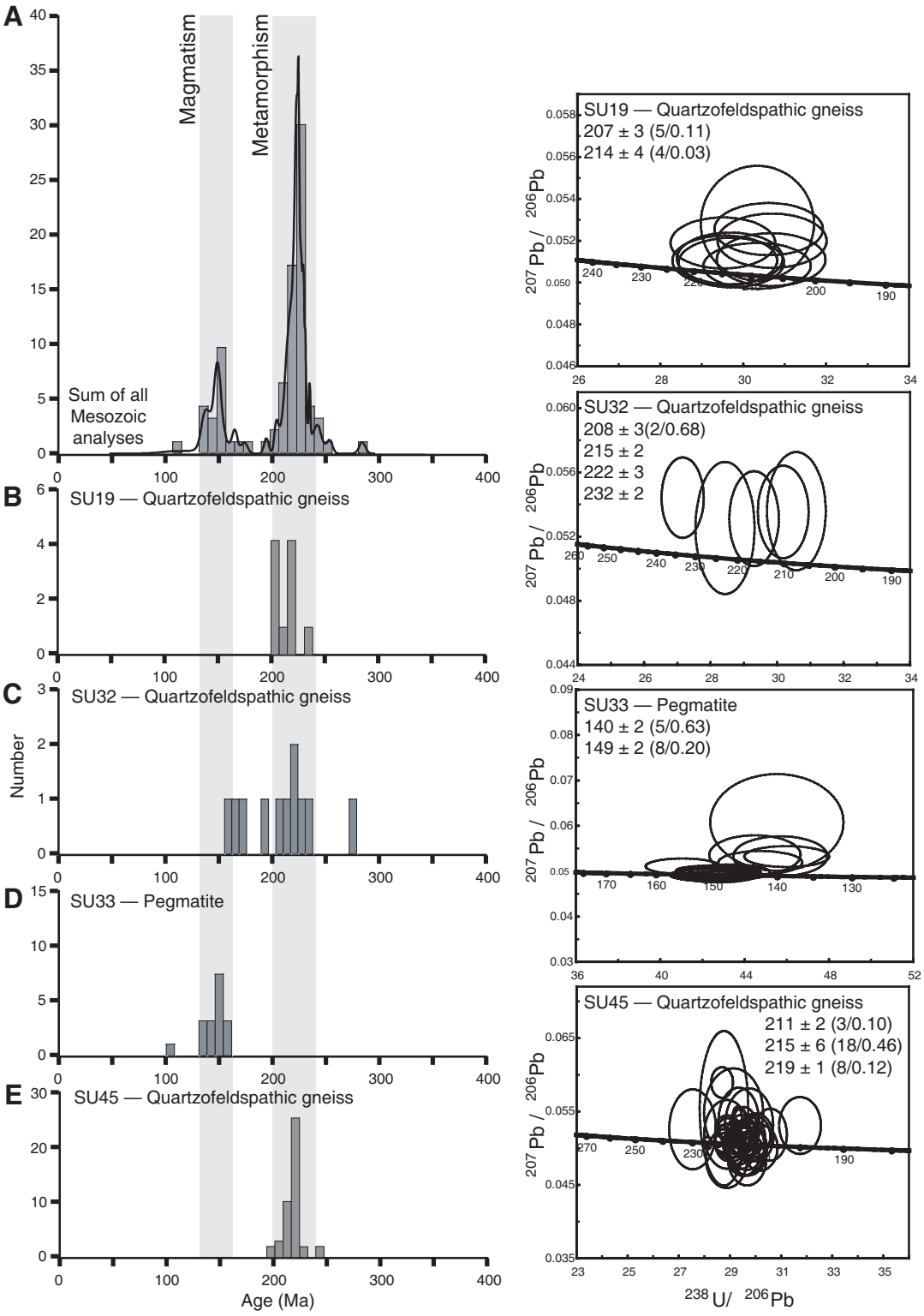

Figure 5. Histogram and probability density curves for (A) summary of Late Permian to Early Cretaceous age data; and (B–E) individual samples SU19, SU32, SU33, and SU45. Samples SU19, SU32, and SU45 record $^{238}U/^{206}Pb$ ages corresponding to ultrahigh-pressure (UHP) and retrograde metamorphism; sample SU33 records melting associated with a later magmatic event. Tera-Wasserburg concordia diagrams show only concordant and near-concordant analyses (data uncorrected for common Pb; error ellipses are 2σ); weighted mean ages for multiple age groups in each sample are listed, with the number of analyses and mean square of weighted deviates (MSWD) included for those averages (in parentheses). Age groups delineated by weighted mean ages were determined based on weighted mean age plots of concordant data (data weighted by 2σ data-point errors; analyses high in common Pb were excluded).

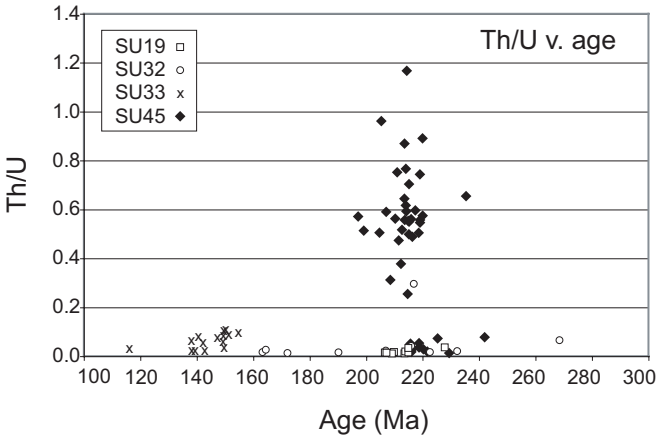

Figure 6. Th-U data for all zircons yielding Mesozoic ages (samples SU19, SU32, SU33, and SU45). This plot shows U-Th data for all Mesozoic data points and includes analyses excluded in weighted mean ages (see discussion in text).

Sample SU29

Sample SU29 is a mylonitized quartzofeldspathic biotite gneiss also from near the central part of the Sulu terrane (locality 37: 35°31′N, 119°08′E; Fig. 1). All U-Pb analyses from sample SU29 yield Late Proterozoic ages between 738 and 786 Ma (concordant analyses only); two subpopulations yield weighted mean ages of 757 ± 10 Ma (4 grains) and 779 ± 6 Ma (7 grains) (Figs. 2B, 3, and 4). The zircon grains are bright with oscillatory zoning under CL, and have Th/U ratios between 0.6 and 2.5 (Appendix 1); later metamorphic zircon growth appears to be absent in this sample. Biotite from SU29 yielded a $^{40}Ar/^{39}Ar$ weighted mean age of 136 ± 1 Ma (Webb et al., this volume).

Samples SU32 and SU33

Quartzofeldspathic gneiss (SU32) and granitic pegmatite vein (SU33) samples are from the Haohung-Taolin area (locality 40: 35°50′N, 119°32′E) near the Yantai-Qingdao-Wulian fault zone along the NW flank of the central dome structure in Sulu (Fig. 1). Samples SU32 and SU33 both record Proterozoic and Mesozoic histories (Figs. 2C–D, 3, and 4). Five concordant Proterozoic analyses from SU32 fall between 701 and 764 Ma, comprising two age groups with weighted mean ages of 704 ± 13 Ma (2 grains) and 760 ± 12 Ma (3 grains). These relict domains are composed of luminescent cores and mantles with oscillatory zoning in CL, and have Th/U ratios between 0.7 and 1.2 (Appendix 1). SU32 gives five concordant analyses with a weighted mean age of 208 ± 3 Ma (2 analyses) and single-grain analyses at 215 ± 2 Ma, 222 ± 3 Ma, and 232 ± 2 Ma (Fig. 2C, 3, and 5). Th/U ratios for the Triassic data fall between 0.01 and 0.04, and come from dark, rounded zircon rims (Fig. 6; Appendix 1).

Sample SU33 yields two concordant ages at 718 ± 17 Ma and 749 ± 14 Ma; these analyses are from a luminescent core and mantle (external to an irregular core) with oscillatory zoning and have Th/U ratios between 0.7 and 1.8 (Figs. 2D and 4; Appendix 1). Late Jurassic to Early Cretaceous spot ages from SU33 yield weighted mean ages of 140 ± 2 Ma (5 grains) and 149 ± 2 (8 grains); these data have Th/U ratios <<0.01 and come from both luminescent rims and nonluminescent cores with oscillatory zoning (Figs. 3, 5, and 6; Appendix 1). White mica from SU33 yields a $^{40}Ar/^{39}Ar$ weighted mean age of 128 ± 1 Ma (Webb et al., this volume).

Sample SU45

Sample SU45 is a quartzofeldspathic biotite gneiss from an island outcrop near Weihai on the Shandong Peninsula (locality 48: 37°31′N, 122°01′E; Fig. 1). Apart from one Early Proterozoic age, this sample yields only Mesozoic data for both luminescent oscillatory-zoned cores and mantles, as well as uniformly nonluminescent, rounded rims (Figs. 2E, 3, and 5). These Mesozoic data have weighted mean ages of 211 ± 2 Ma (3 grains), 215 ± 6 Ma (18 grains), and 219 ± 1 Ma (8 grains) and unusually high Th ratios (0.01–1.2) compared to other metamorphic zircons in this study (Fig. 6; Appendix 1). Biotite from sample SU45 produced a $^{40}Ar/^{39}Ar$ weighted mean age of 70 ± 2 Ma (Webb et al., this volume).

RARE EARTH ELEMENT ANALYSES OF TRIASSIC ZIRCON DOMAINS

Rare earth element (REE) data were collected using the SHRIMP-RG in the same analysis spots for which U-Pb dating was done in an attempt to distinguish between eclogite-facies zircon growth and lower-grade metamorphic zircon growth.

Analytical Technique

The lack of well-characterized zircon crystals for REE calibration standards requires calibration to other REE and zircon standards. For our analyses, we calibrated to NIST SRM 611 and NIST SRM 613 (REE-spiked) glasses; SL13 standard zircon (REE concentrations based on SL13-LA-CH in Hoskin, 1998); and CZ3 (U-concentration standard). NIST glasses and SL13 zircon were analyzed at the beginning and end of the SHRIMP session. Rare earth data were collected in three scans, with the CZ3 standard repeated after every twelfth analysis; multiple CZ3 and SL13 standards were run before and after each sample. Details of data reduction were as described by Hoskin (1998); data were normalized to the chondrite values of McDonough and Sun (1995).

Summary and Interpretation of REE Data

Three samples analyzed for REEs (SU19, SU32, SU45) show consistent patterns of depleted light (L) REEs, with pronounced positive Ce anomalies and enriched heavy (H) REEs with respect to middle (M) REEs (Fig. 7). Figure 7 shows REE patterns for zircons yielding Triassic ages in core-mantle and

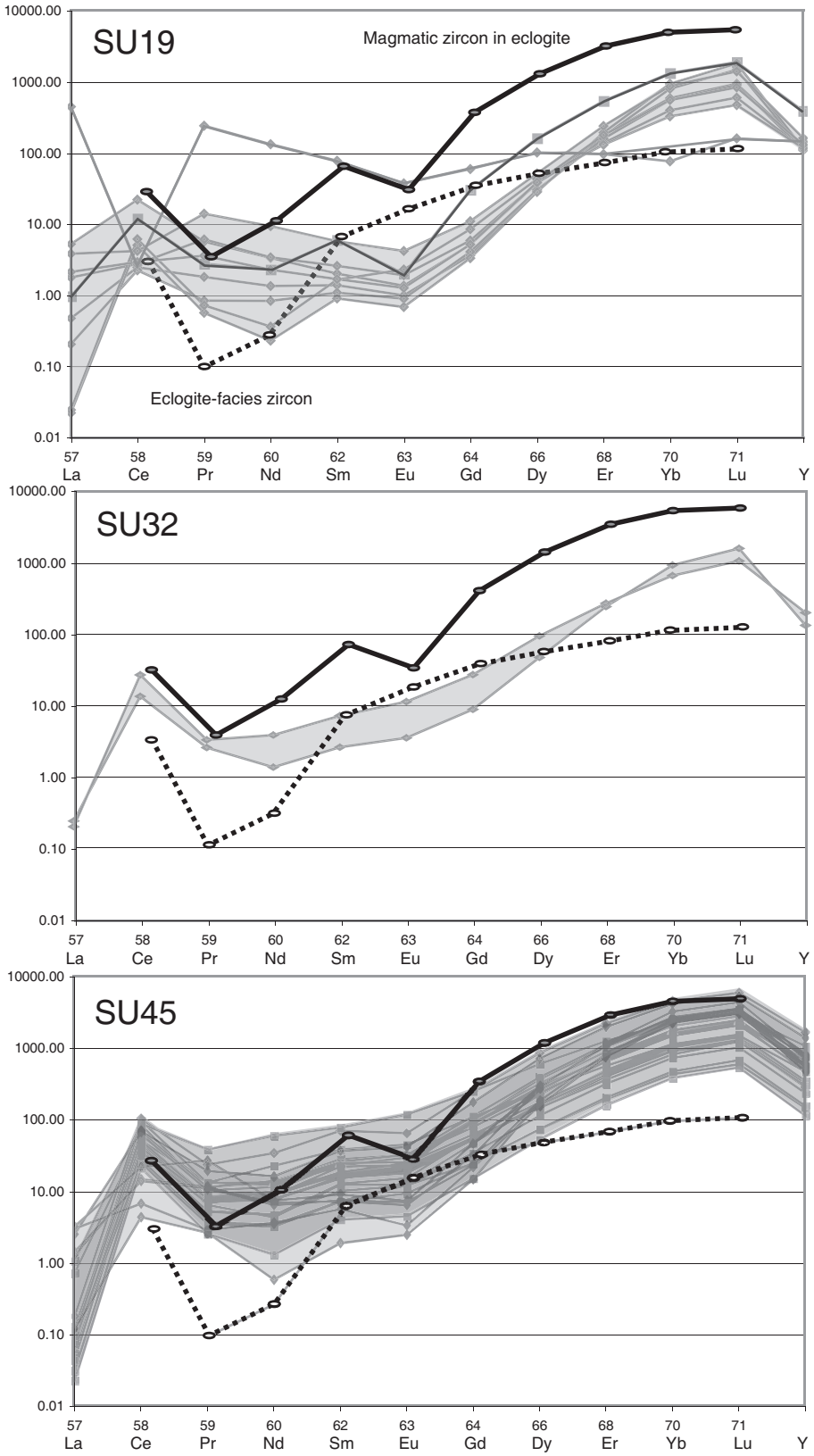

Figure 7. Chondrite-normalized (McDonough and Sun, 1995) rare earth element (REE) patterns of zircons yielding Mesozoic U-Pb ages for cores-mantles (dark-gray lines and fields) and rims (light-gray lines and fields) for samples SU19, SU32, and SU45. Heavy solid black and dashed black lines show typical patterns for magmatic zircon and eclogite-facies zircon, respectively (from Rubatto and Hermann, 2003).

rim growth domains (see also Fig. 3). In general, core-mantle analyses give a broader range of LREE values and a smaller range of HREE values, whereas rim analyses show a smaller range of LREEs and a broader range of HREE values.

A single-rim analysis for sample SU19 shows a pronounced Eu anomaly, whereas core-mantle analyses show only a slight Eu anomaly; both core-mantle and rim analyses have an enriched HREE signature compared to the MREEs (two analyses with negative Ce anomalies and very different REE patterns were ignored because these analyses may have sampled inclusions within zircon). Rim analyses for SU32 lack a Eu anomaly and show enrichment in HREEs. Despite the relatively high Th/U ratios for SU45 (resulting from relatively high Th concentrations; Fig. 6 and Appendix 1), the REE patterns for this sample are comparable to SU19 and SU32. In sample SU45, the core-mantle analyses lack a negative Eu anomaly, while rim analyses show only a slight negative Eu anomaly. Ages corresponding to these zircon core-mantle and rim domains span the entire period of metamorphism from ca. 230 to 200 Ma; i.e., rim ages are not systematically younger than mantle ages and have no apparent correlation to any particular age group (see following).

Zircon growing in the presence of garnet should show a depleted HREE pattern, because garnet preferentially incorporates HREEs (see example from Rubatto and Hermann [2003] in Fig. 7). In contrast, magmatic zircon grown in the presence of plagioclase should have elevated HREEs and a negative Eu anomaly (example in Fig. 7; Hermann et al., 2001; Rubatto, 2002; Rubatto and Hermann, 2003).

Our age and REE data for zircons are from quartzofeldspathic gneisses that have abundant feldspar and only rare to minor garnet, consequently, the REE patterns are generally consistent with zircon growing in association with feldspar. These REE patterns do not rule out zircon crystallization at eclogite-facies conditions in a largely garnet-free rock, but may in fact reflect zircon growth at amphibolite-facies conditions based on our interpretation of the age data for these samples.

DISCUSSION OF NEW U-Pb SHRIMP DATING

Zircon records a long history of events during the evolution of the Sulu terrane. Relict zircon domains preserve protolith ages (Fig. 4), and newer zircon growth and recrystallization record metamorphism from UHP conditions during retrogression (Figs. 5 and 8), and mark the early stages of melting (Fig. 5) during a widespread magmatic event.

Proterozoic Protolith Ages and Yangtze Craton Affinity

The location of the suture between the Yangtze and Sino-Korean cratons has been a matter of significant debate, and U-Pb dating of zircon is helping to piece together the Precambrian history of this region (e.g., Hacker et al., 1998; B.R. Hacker, 2005, personal commun.); Faure et al., 2001, 2003; Grimmer et al., 2003; Wu et al., 2004; Zheng et al., 2004a; Ratschbacher et al., this volume; B.R. Hacker (2005, personal commun.). The predominance of ages between 650 and 850 Ma is used to identify the Yangtze craton, and the absence of these ages (locally the presence of 400–480 Ma ages) signifies a Sino-Korean craton affinity (Hacker et al., 1998). Zircon cores and mantles from four different samples in this study produced ages between 700 and 790 Ma (Fig. 4; Appendix 1), strengthening earlier interpretations that the Sulu gneiss belongs to the Yangtze craton. In the Sulu area, the location of the suture has conventionally been placed along the Yantai-Qingdao-Wulian fault, based on the differences in the geology to the southeast and northwest of the fault, where the UHP Sulu gneiss marks the northern extent of the Yangtze craton (Fig. 1). Faure et al. (2001, 2003) more recently suggested that the suture lies northwest of the Yantai-Qingdao-Wulian fault, based on similarities in deformational style, the presence of migmatites, and a granulite-facies overprint across the fault. New dating (Wu et al., 2004; B.R. Hacker (2005, personal commun.) supports this by showing that some high-grade rocks northwest of the Yantai-Qingdao-Wulian fault do have ca. 750 Ma ages. B.R. Hacker (2005, personal commun.) interpreted this to mean that the Sulu area northwest of the Yantai-Qingdao-Wulian fault is part of the Qinling microcontinent, which rifted from the Yangtze craton (Ratschbacher et al., this volume) during the breakup of Rodinia and was not subducted during the Triassic UHP orogeny.

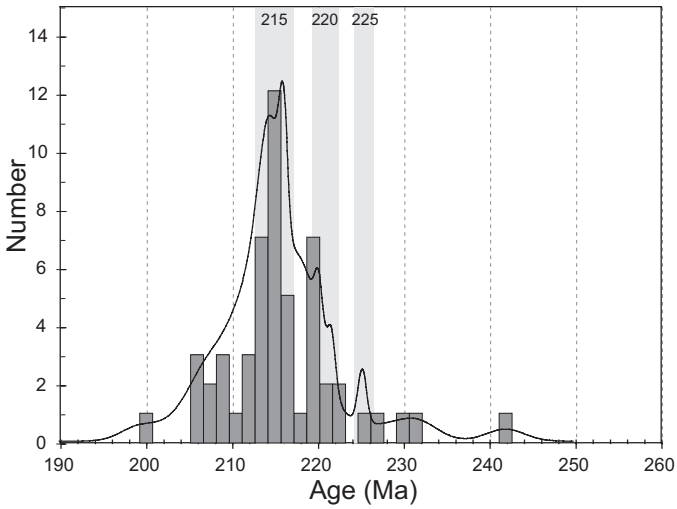

Figure 8. Histogram and probability density curve for all concordant single-grain ages between 250 and 200 Ma from samples SU19, SU32, and SU45. Major age groups recorded in zircon fall around 220 Ma and 215 Ma.

Cretaceous Magmatism

Dating of a pegmatite vein (sample SU33) near the Yantai-Qingdao-Wulian fault zone yields weighted mean ages between ca. 140 and 150 Ma using concordant single-grain ages from

138 ± 2 Ma to 155 ± 3 Ma (Fig. 5). These ages slightly overlap the 137–126 Ma ages of undeformed igneous rocks in northern Dabie (Ratschbacher et al., 2000), and may reflect an early stage of related melting.

Triassic UHP and Retrograde Metamorphism

Concordant single-grain ages for this study range from ca. 240 Ma to 200 Ma, with probability density curve peaks at ca. 225 Ma, 220 Ma, and 215 Ma (Fig. 8); there were an insufficient number of spot analyses older than 220 Ma (Appendix 1) to define distinct age groups apart from what is seen in the probability density curve in Figure 8. These age groups are indistinguishable on the basis of their U-Th-Pb concentrations, Th/U ratios, grain morphology, CL images, or REE patterns. The age of UHP metamorphism in the Sulu terrane has been estimated between ca. 220 and 230 Ma, based on dating of coesite-bearing domains in zircon (Yang et al., 2003; Liu et al., 2004b), a disparity of 10 m.y.; combining all the individual attempts to date UHP metamorphism (Fig. 9), instead of relying on a single "best" study, may reveal a more reliable date. Based on the distribution of all Sulu ages shown in Figure 9, the ages in this study all date synexhumation retrograde metamorphism—apart from a few single-grain ages ca. 230 Ma that may record UHP metamorphism. This interpretation is further supported by the $^{40}Ar/^{39}Ar$ dating presented in Webb et al. (this volume), suggesting amphibolite- to upper greenschist–facies metamorphism at ca. 213 Ma in some of the same samples. Many of the ages reported from high-temperature thermochronometry for the Hong'an–Dabie and Sulu areas span both peak and retrograde metamorphism (Fig. 9; Appendices 2 and 3). In fact, the distribution of ages seen in Figure 9 suggests that it is perhaps more accurate to describe these ages as recording a period of metamorphism beginning with peak *P-T* conditions and continuing through the initial exhumation.

There are many examples of low- to intermediate-temperature zircon crystallization, including amphibolite-facies zircon growth in UHP rocks from the Kokchetav Massif (Hermann et al., 2001). Hermann et al. (2001) showed that UHP eclogite-facies zircon (identified by the presence of coesite and diamond) have U-Th-Pb concentrations and cathodoluminescence that are identical to upper amphibolite– to granulite-facies zircon. Metamorphic recrystallization of zircon rims at post-peak amphibolite-facies conditions may result from dehydration reaction–derived fluids during exhumation (Hermann et al., 2001; Leech, 2001); the intermittent presence of these fluids could allow zircon (re)crystallization during exhumation during changing *P-T* conditions.

Yang et al. (2003) and Liu et al. (2004b) produced weighted mean ages for coesite-bearing domains in zircon (mantles) of 221 ± 12 Ma for eclogite in peridotites and 231 ± 4 Ma for host gneisses, respectively, and interpreted these ages as the time of UHP metamorphism. Liu et al. (2004b) compared those ages with ages from quartz-bearing zircon rims and calculated a weighted mean age of 211 ± 4 Ma for the amphibolite-facies overprint. We have not identified coesite and/or diamond within our dated zircon that would enable interpretations like Yang et al. (2003) and Liu et al. (2004b), but the Th/U ratios for our zircons are on par with metamorphic zircons from other Sulu gneiss samples (e.g., 0.01–0.8 from Liu et al. [2004b] compared to <<0.01–1.2 from this study). While this is an excellent approach, the data of Yang et al. (2003) and Liu et al. (2004b) suffer from some problems that we discuss in the following; a better approach is to look at all dates for Sulu as a whole (Fig. 9).

Timing of UHP Metamorphism in the Dabie-Sulu Orogen

Results of U-Pb SHRIMP dating of zircon from the Sulu gneiss in this study are representative of all the high-temperature thermochronology for Sulu (compare Figs. 8 and 9A). Figure 9 compares all published high-temperature geochronology (U-Pb, Pb-Pb, Pb-Th, Sm-Nd, and Rb-Sr) for both the Sulu (including this study) and Hong'an–Dabie areas that attempt to date UHP metamorphism (details of the data included in Figure 9 are in Appendices 2 and 3); $^{40}Ar/^{39}Ar$ analyses have been specifically excluded, because these dates record cooling through temperatures well below UHP conditions (e.g., ~350 °C for muscovite and ~450 °C for phengite; MacDougall and Harrison, 1988). Histograms of these ages in Figures 9A (Sulu) and 9E (Dabie–Hong'an) span similar ranges (broadly 260–200 Ma), but the probability density curves for each data set define different age populations. The dominant age groups for analyses from Sulu fall around 229 Ma, 219 Ma, and 207 Ma, while they are ~10 m.y. older in the Dabie–Hong'an areas (240 Ma, 228 Ma, and 216 Ma).

Outliers in the data displayed in the histograms in Figure 9 may be explained in several ways: A few of the older ages come from analyses of zircons from ultramafic rocks or eclogite within ultramafic rocks that may not have experienced the same *P-T-t* history as the UHP rocks within the Sulu gneiss (e.g., 242 ± 8 Ma from zircons in dunite from Sulu; Zhao et al., this volume); several are concordia intercept ages with large uncertainties (e.g., 258 ± 25 Ma; Zheng et al., 2004b); several are lower intercept ages from very discordant data (e.g., the 228 ± 29 Ma date of Yang et al., 2003); and some are weighted mean ages with high mean square of weighted deviates (MSWD) values (e.g., 2.2 for a 208 ± 4 Ma age for a paragneiss from Liu et al., 2004b).

Based on the summary of the dating for both the Sulu and Hong'an–Dabie areas shown in Figure 9, and taking into account the problems described above, we suggest that UHP metamorphism took place at ca. 230 Ma in Sulu and at ca. 240 Ma in Hong'an–Dabie area, and that all younger dates represent retrograde metamorphism during exhumation.

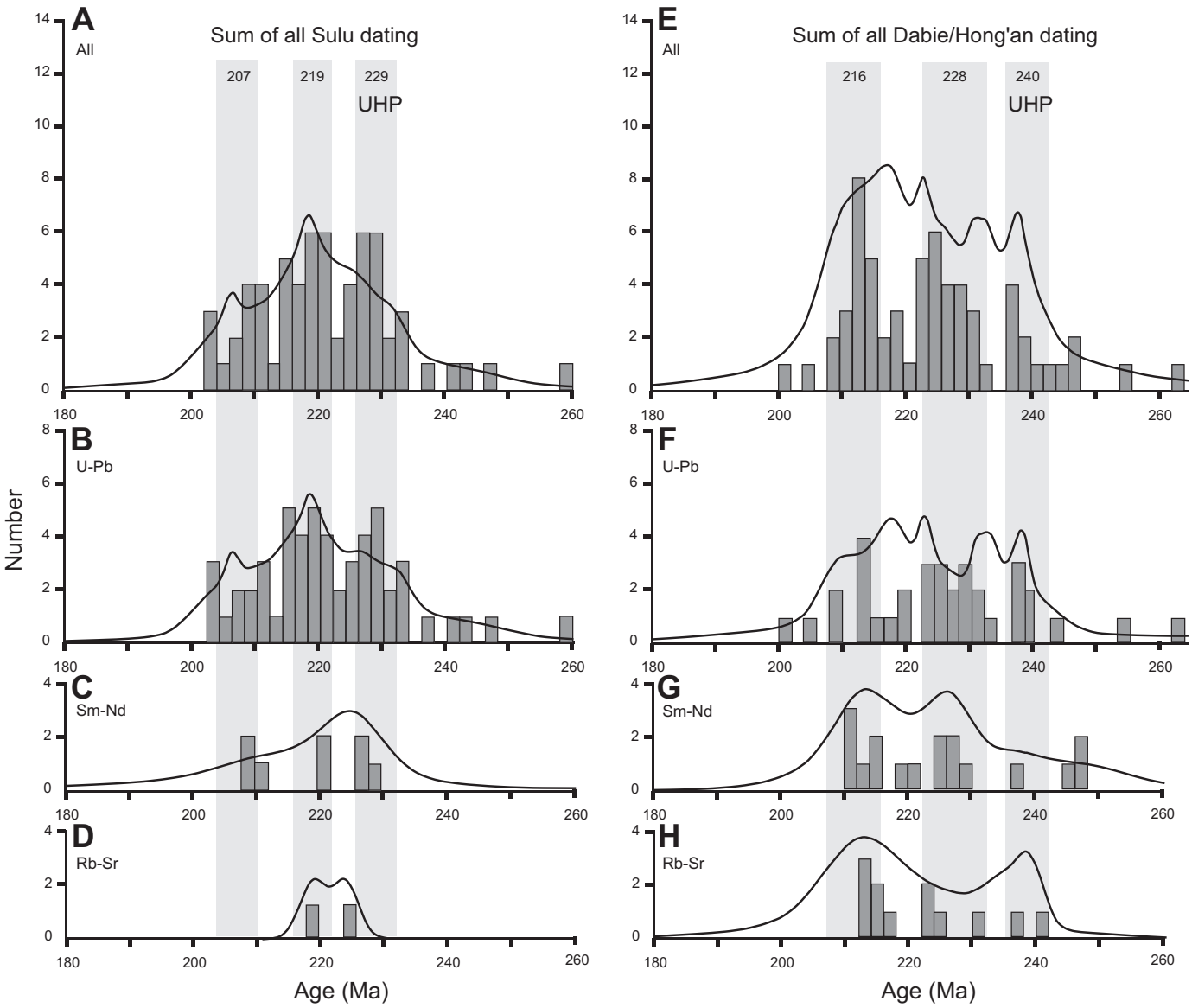

Figure 9. Histograms and probability density curves for all high-temperature thermochronometry for the Sulu and Dabie–Hong'an areas representing Triassic ultrahigh-pressure (UHP) to Early Jurassic retrograde metamorphism. A and E summarize all ages for Sulu and Dabie, respectively; B and F show only U-Pb ages (with a few Pb-Pb and Th-Pb dates); C and G show only Sm-Nd data; and D and H contain Rb-Sr data. Age groups from multiple chronometers marked with gray bands show that the Dabie–Hong'an area experienced UHP metamorphism at ca. 240 Ma, as much as 15 m.y. earlier than the Sulu area. Ages that have error estimates <±30 m.y. from all published high-temperature geochronology for the Hong'an, Dabie, and Sulu areas between 260 and 200 Ma are included (the likely age range for peak and retrograde metamorphism). Data include published weighted mean ages, lower intercept ages on concordia plots, and single-grain ages where the weighted mean ages or intercept ages were not available; weighted mean ages were calculated when possible for large numbers of published single-grain ages (e.g., Wallis et al., 2005) to avoid weighting single-grain ages too heavily. *Isoplot* was used to produce the histograms and probability density curves from the data presented in Appendices 2 and 3. Data for Sulu are from Li et al. (1993, 1999); Ames et al. (1996); Rumble et al. (2002); Zheng et al. (2002, 2004b); Yang et al. (2003); Liu et al. (2004a, 2004b); Wallis et al. (2005); Yang et al. (2005); Zhao et al. (2005); B.R. Hacker (2005, personal commun.); Zhao et al. (this volume); and this study. Data from the Dabie–Hong'an areas are from Ames et al. (1993, 1996); Li et al. (1993, 1999); Okay et al. (1993); Chavagnac and Jahn (1996); Bruguier et al. (1997); Rowley et al. (1997); Hacker et al. (1998, 2000); Maruyama et al. (1998) cit. in Hacker and Wang (1995); Ayers et al. (2002); Chen et al. (2003); Grimmer et al. (2003); Zheng et al. (2003, 2004b); Li et al. (2004); and Liu et al. (2004c).

REVISED MODEL FOR COLLISION, SUBDUCTION, AND UHP METAMORPHISM

There are significant implications for orogen-scale development if UHP metamorphism occurred in the Dabie–Hong'an area 10 m.y. before Sulu reached UHP conditions. Models like B.R. Hacker (2005, personal commun.) that assume uniform timing of UHP metamorphism in the Dabie and Sulu areas are potentially flawed in light of evidence from this study, which suggests that they may have had separate, though related, orogenic histories.

Traditionally, it has been assumed that reversing strike-slip motion along the Tan-Lu fault would restore Sulu to its original orogenic position adjacent to Dabie and that UHP metamorphism took place simultaneously east and west of the Tan-Lu fault. Assuming therefore that structures in both the Hong'an–Dabie and Sulu areas would be parallel if they had a common history, Webb et al. (2002) described a model whereby Sulu must have rotated ~25° counterclockwise during offset along the Tan-Lu fault. These simplified views contrast with more complex models: Hacker et al. (2000, 2004) described a detailed model for subduction and exhumation of the Dabie–Hong'an area based on paleomagnetic data, which suggest 60° of clockwise rotation during exhumation of a subducted wedge-shaped or Florida-like promontory. But this model did not account for differences in the timing of UHP metamorphism and exhumation in the Sulu area.

The tectonic evolution of the Dabie-Sulu belt is greatly simplified if we use a model that does not require contiguity between Sulu with Dabie and allows a 10 m.y. time difference for UHP metamorphism in Sulu and Dabie; both are more consistent with the rotational exhumation model of Hacker et al. (2000, 2004). Dabie–Hong'an and Sulu were certainly part of the same deeply subducted leading edge of the Yangtze craton, but perhaps they were not adjacent parts of the Yangtze craton (see Figure 5 in Hacker et al., 2004). The summary of the dating from the two areas shown in Figure 9 suggests that the Dabie area was the first to be subducted to UHP depths; this may have resulted from the irregular shape of either or both of the Sino-Korean or Yangtze cratons. In order to honor the rotational exhumation model suggested by paleomagnetic data, Dabie may have resided at UHP depths until ca. 230 Ma, when a crustal delamination/slab breakoff event (Leech, 2001; Leech et al., 2005) or a buoyancy-induced tear between oceanic and continental crust (Hacker et al., 2000, 2004) beginning in the east in Sulu triggered exhumation. Alternatively, rotational exhumation of Dabie–Hong'an began first, entirely separate from Sulu, and different exhumation processes for the two areas were not linked (i.e., Sulu did not participate in the clockwise rotational exhumation and was a separate UHP slab returned to the surface). Some of the ~25° of rotation required to restore structures in Sulu parallel to Dabie may not be due to rotation during translation along the Tan-Lu fault, but rather can be explained by a separate collision-exhumation history.

ACKNOWLEDGMENTS

We thank Joe Wooden, Frank Mazdab, Chris Mattinson, and Bob Jones for help with sample preparation, data analysis and reduction. This research is supported by a grant to J.G. Liou at Stanford University (National Science Foundation grant EAR-0003355). Many thanks are due to Bill McClelland, Brad Hacker, Trevor Ireland, Jeremy Hourigan, and one anonymous reviewer for helpful suggestions that improved an earlier version of this manuscript.

APPENDIX 1. U-Th-Pb DATA FOR ALL SHRIMP ANALYSES OF ZIRCON

Analysis spot	U (ppm)	Th (ppm)	Th/U	$^{204}Pb/^{206}Pb^{*}$	$^{206}Pb^{\dagger}$ (%)	$^{238}U/^{206}Pb^{*}$		$^{207}Pb/^{206}Pb^{*}$		$^{207}Pb/^{235}U^{\#}$		$^{206}Pb/^{238}U$ Age† (Ma)	
SU19-1	1898	15	0.01	0.0000	0.2	30.6735	1.7469	0.0511	1.0079	0.2282	2.0663	206.5	3.6
SU19-2	2460	22	0.01	0.0001	0.1	30.3359	1.7423	0.0508	0.8809	0.2261	2.1018	208.9	3.6
SU19-3	587	3	0.01	0.0001	0.4	30.3410	1.8384	0.0528	2.1187	0.2330	3.1582	208.3	3.8
SU19-4	1885	47	0.03	0.0000	0.2	29.5095	1.7472	0.0519	0.9584	0.2395	2.0869	214.3	3.7
SU19-5	2137	20	0.01	0.0001	0.1	29.7114	1.7461	0.0510	0.9457	0.2312	2.1537	213.2	3.7
SU19-6	2671	78	0.03	0.0000	0.3	27.7805	1.7385	0.0526	0.7900	0.2604	1.9299	227.3	3.9
SU19-7	467	393	0.87	0.0001	0.6	10.1257	1.7811	0.0643	1.0424	0.8636	2.1536	603.8	10.5
SU19-8	1872	20	0.01	0.0002	0.3	30.6140	1.7451	0.0526	0.9680	0.2260	2.4470	206.5	3.6
SU19-9	1861	24	0.01	0.0001	0.1	29.6783	1.7557	0.0512	0.9868	0.2336	2.1437	213.3	3.7
SU19-10	2153	21	0.01	0.0001	0.3	30.6956	1.7512	0.0520	1.0178	0.2275	2.3186	206.1	3.6
SU19-11	335	95	0.29	0.0001	0.6	12.1349	1.8084	0.0623	1.3455	0.6923	2.3567	507.3	9.0
SU19-12	180	127	0.73	0.0003	0.5	8.3492	1.8647	0.0674	1.4999	1.0304	3.5042	725.6	13.2
SU19-13	2156	20	0.01	0.0000	0.1	29.5558	1.7469	0.0511	0.9524	0.2347	2.0277	214.2	3.7
SU19-14	345	237	0.71	0.0000	0.6	9.9626	1.7980	0.0644	1.1980	0.8862	2.3322	613.3	10.8
SU19-15	601	336	0.58	0.0002	0.8	13.8890	1.7728	0.0622	1.2212	0.5843	2.7136	444.6	7.7
SU19-16	241	158	0.68	0.0001	0.4	10.3046	1.8321	0.0629	1.4749	0.8248	2.5429	594.6	10.6
SU19-17	124	83	0.69	0.0000	0.4	8.0100	1.9221	0.0670	1.9022	1.1415	2.7917	755.8	14.1
SU19-18	241	211	0.90	0.0001	0.5	9.1980	1.8392	0.0653	1.6477	0.9464	2.9336	662.1	11.9
SU19-19	392	266	0.70	0.0001	0.4	9.2606	1.7865	0.0645	1.0657	0.9438	2.1854	658.4	11.4
SU19-20	533	411	0.80	0.0000	0.1	7.9790	1.7764	0.0651	0.9250	1.1212	2.0202	760.3	13.1
SU19-21	104	119	1.18	0.0002	0.4	8.3599	1.9849	0.0664	2.3313	1.0508	3.6901	725.6	14.0
SU19-22	1871	680	0.38	0.0002	0.9	15.4351	1.7466	0.0618	0.6670	0.5255	2.1908	401.0	6.9
SU19-23	96	131	1.40	0.0000	0.3	8.1229	1.9694	0.0665	2.1051	1.1273	3.2234	746.0	14.3
SU19-24	285	182	0.66	0.0001	0.0	7.9127	1.8107	0.0641	1.1848	1.1018	2.2670	767.4	13.5
SU19-25	793	1335	1.74	0.0000	0.2	8.1420	1.7525	0.0652	0.7134	1.0988	1.8996	745.5	12.7
SU19-26	472	344	0.75	0.0001	0.3	8.3258	1.7884	0.0657	1.0586	1.0550	2.3334	729.1	12.7
SU19-27	317	201	0.66	0.0001	0.4	8.6553	1.7999	0.0659	1.2512	1.0119	2.5349	702.0	12.3
SU29-1	192	475	2.55	0.0000	0.3	7.9574	1.0348	0.0669	1.4183	1.1625	1.7608	760.7	7.7
SU29-2	79	131	1.71	0.0003	0.5	7.6702	1.3222	0.0690	2.1586	1.1594	3.1251	786.3	10.2
SU29-3	85	82	1.00	0.0002	1.3	9.1091	1.4564	0.0720	2.2929	1.0415	3.5682	663.1	9.5
SU29-4	271	238	0.91	0.0000	0.2	7.7728	0.9592	0.0662	1.1993	1.1762	1.5390	778.8	7.3
SU29-5	52	82	1.63	0.0002	0.6	7.7379	1.5354	0.0699	2.6912	1.1889	3.7664	778.8	11.7
SU29-6	34	42	1.28	–0.0001	0.7	8.1884	1.8617	0.0688	4.4423	1.1759	4.8471	738.2	13.6
SU29-7	61	99	1.67	0.0006	1.2	7.9744	1.4567	0.0739	2.4241	1.1194	5.8958	752.8	10.8
SU29-8	34	44	1.33	0.0005	0.4	7.9100	1.7938	0.0675	3.3885	1.0292	7.5977	764.5	13.5
SU29-9	1415	2050	1.50	0.0001	0.6	9.8775	0.8051	0.0648	0.5919	0.8892	1.1007	618.1	4.9
SU29-10	58	88	1.57	0.0000	0.1	7.7614	1.4669	0.0653	2.6126	1.1601	2.9947	780.8	11.2
SU29-11	76	107	1.46	–0.0001	0.7	8.0239	1.3188	0.0692	3.4033	1.2178	3.5886	752.5	9.9
SU29-12	122	121	1.03	0.0009	1.5	9.3908	1.2302	0.0730	2.1728	0.8654	7.1115	643.0	7.9
SU29-13	225	207	0.95	0.0001	0.3	7.7250	1.0102	0.0675	1.2984	1.1735	1.7369	782.3	7.7
SU29-14	174	222	1.32	0.0000	0.5	7.8299	1.0625	0.0685	1.5027	1.2195	1.8323	771.2	8.0
SU29-15	142	138	1.01	0.0002	0.3	7.7478	1.1123	0.0672	1.6485	1.1364	2.8222	780.4	8.5
SU29-16	33	21	0.66	0.0015	2.4	8.4680	1.9098	0.0821	3.3147	0.9533	13.6165	703.2	13.4
SU32-1	55	44	0.83	0.0002	1.1	13.7353	1.6217	0.0641	3.5605	0.6177	4.4902	448.4	7.3
SU32-2	65	57	0.91	0.0001	0.9	8.5516	1.3864	0.0701	2.7590	1.1171	3.1589	706.7	9.7
SU32-3	59	39	0.69	0.0002	1.0	11.4911	1.5387	0.0658	3.1408	0.7580	3.7360	532.8	8.1
SU32-4	55	82	1.55	0.0001	0.7	8.8687	1.5481	0.0676	3.5438	1.0176	4.1282	684.2	10.5
SU32-5	108	60	0.57	0.0013	2.6	16.5861	1.2486	0.0745	2.4257	0.4485	11.0030	367.9	4.7
SU32-6	283	6	0.02	0.0002	0.5	38.7042	1.2058	0.0526	3.1989	0.1779	4.2483	163.7	2.0

(continued)

APPENDIX 1. U-Th-Pb DATA FOR ALL SHRIMP ANALYSES OF ZIRCON *(continued)*

Analysis spot	U (ppm)	Th (ppm)	Th/U	$^{204}Pb/^{206}Pb^{*}$	$^{206}Pb^{\dagger}$ (%)	$^{238}U/^{206}Pb^{*}$		$^{207}Pb/^{206}Pb^{*}$		$^{207}Pb/^{235}U^{\#}$		$^{206}Pb/^{238}U$ Age† (Ma)	
SU32-7	91	102	1.15	0.0002	0.2	7.9823	1.2150	0.0661	1.9054	1.0971	2.5113	759.1	9.0
SU32-8	28	21	0.79	0.0013	2.3	11.9807	1.8616	0.0759	5.0588	0.6393	12.6867	505.2	9.6
SU32-9	17	13	0.80	–0.0005	0.2	8.0738	2.2241	0.0657	4.5446	1.2488	4.8177	751.1	16.4
SU32-10	375	5	0.01	0.0001	0.0	33.5185	0.9925	0.0494	2.1737	0.1994	2.4749	189.5	1.9
SU32-11	484	16	0.03	0.0001	1.0	19.4926	0.8984	0.0600	1.3216	0.4150	1.8145	319.5	2.9
SU32-12	867	314	0.37	0.0001	0.6	10.5356	0.8256	0.0638	0.8952	0.8194	1.5299	581.2	4.7
SU32-13	67	71	1.10	–0.0001	0.2	7.9266	1.3067	0.0659	2.1967	1.1782	2.5277	764.4	9.8
SU32-14	431	27	0.06	0.0005	0.4	23.4001	0.9477	0.0545	1.7145	0.2799	5.1917	268.7	2.5
SU32-15	437	17	0.04	0.0003	0.7	20.8003	0.9490	0.0579	1.6091	0.3485	3.5527	300.5	2.8
SU32-16	1078	992	0.95	0.0002	0.8	9.4441	0.8077	0.0670	0.6001	0.9265	1.4495	644.1	5.1
SU32-17	428	8	0.02	0.0006	0.5	30.5808	1.1790	0.0536	2.8053	0.2008	9.0147	206.5	2.4
SU32-18	301	213	0.73	0.0000	0.5	10.5877	0.9469	0.0627	1.3719	0.8247	31.8449	579.2	5.4
SU32-19	116	34	0.30	0.0014	3.3	28.2986	1.6846	0.0762	5.4794	0.2619	19.2006	216.7	3.9
SU32-20	324	13	0.04	0.0002	0.4	29.3074	1.0377	0.0531	2.2773	0.2387	2.8531	215.5	2.2
SU32-21	64	52	0.83	0.0023	3.6	15.9276	1.6211	0.0826	2.9260	0.4003	29.1435	378.9	6.4
SU32-22	488	7	0.01	0.0003	0.3	28.4342	1.2765	0.0525	3.2036	0.2352	6.7931	222.2	2.8
SU32-24	60	49	0.85	0.0000	0.6	8.6519	1.3299	0.0672	2.2918	1.0713	2.6499	701.1	9.2
SU32-25	159	67	0.44	0.0002	1.0	15.2005	1.0803	0.0629	1.9786	0.5366	3.3422	406.6	4.4
SU32-26	35	26	0.77	–0.0009	1.7	12.4316	1.7073	0.0704	3.5655	0.9380	9.3153	490.6	8.4
SU32-27	73	22	0.32	0.0004	1.3	11.1336	1.3126	0.0686	2.4665	0.7695	4.2075	547.6	7.2
SU32-28	284	78	0.28	0.0002	1.3	11.2416	0.9337	0.0684	1.1871	0.7983	2.3174	542.6	5.0
SU32-29	221	3	0.01	0.0018	2.1	38.3570	1.7368	0.0658	4.8652	0.1360	28.0786	162.4	2.9
SU32-30	869	55	0.06	0.0000	0.7	11.9410	0.8684	0.0628	0.9124	0.7169	1.3920	515.0	4.4
SU32-31	129	1	0.01	0.0006	1.5	36.5541	1.4229	0.0613	5.6690	0.1951	7.8256	171.4	2.6
SU32-32	455	7	0.02	0.0002	0.5	27.1594	0.9553	0.0544	1.8810	0.2625	3.5521	231.9	2.2
SU32-33	414	5	0.01	0.0003	0.4	30.1851	1.0351	0.0535	2.1987	0.2248	5.1057	209.2	2.2
SU33-1	1097	42	0.04	0.0005	0.6	46.0014	1.7861	0.0532	1.7686	0.1372	5.0837	137.8	2.5
SU33-2	1506	81	0.06	0.0001	0.1	43.3190	1.7664	0.0498	1.4061	0.1550	2.4065	146.9	2.6
SU33-3	3383	288	0.09	0.0000	0.0	42.5381	1.7400	0.0488	0.9143	0.1575	1.9775	149.8	2.6
SU33-4	2460	167	0.07	0.0000	0.1	42.2755	1.7473	0.0492	1.0679	0.1589	2.0995	150.6	2.6
SU33-5	15	1	0.06	0.0200	25.9	33.7215	4.4753	0.2545	7.4224	N/A	N/A	140.1	9.8
SU33-6	3736	261	0.07	0.0002	0.3	41.0529	1.7381	0.0511	1.3694	0.1636	2.5904	154.7	2.7
SU33-7	1442	56	0.04	0.0001	0.1	42.7582	1.7701	0.0493	1.4467	0.1545	2.5282	148.9	2.6
SU33-8	3148	256	0.08	0.0000	0.2	42.5688	1.7421	0.0501	0.9463	0.1605	2.0697	149.4	2.6
SU33-9	5	0	0.00	0.0313	19.9	44.3753	7.0797	0.2059	23.2853	N/A	N/A	115.3	12.4
SU33-10	692	20	0.03	0.0000	0.4	44.7452	1.8176	0.0519	2.0012	0.1599	2.7031	141.9	2.6
SU33-11	226	0	0.00	0.0003	0.6	45.7001	1.9959	0.0533	3.3664	0.1479	5.7895	138.7	2.8
SU33-12	35	27	0.80	0.0002	0.4	8.4564	2.3971	0.0659	3.4622	1.0162	4.9377	717.9	16.8
SU33-13	3136	218	0.07	0.0000	0.1	42.4252	1.7422	0.0494	0.9621	0.1593	2.1065	150.0	2.6
SU33-14	247	0	0.00	0.0003	0.6	44.4930	1.9899	0.0536	3.3171	0.1533	5.6095	142.4	2.8
SU33-15	35	0	0.01	0.0087	6.8	39.7503	3.2795	0.1026	11.2161	N/A	N/A	149.4	5.5
SU33-16	1909	87	0.05	0.0000	0.1	42.9270	1.7562	0.0496	1.2079	0.1573	2.1637	148.3	2.6
SU33-17	81	74	0.94	–0.0001	1.0	11.3090	2.1816	0.0656	2.7010	0.8145	3.4424	541.2	11.6
SU33-18	54	0	0.00	0.0024	1.5	45.5307	2.8384	0.0608	7.1638	0.0683	74.8228	137.9	4.0
SU33-19	143	247	1.78	0.0001	0.5	8.0722	1.8849	0.0676	1.6278	1.1182	2.7048	749.6	13.7
SU33-20	89	124	1.44	0.0008	2.1	9.2895	2.1001	0.0782	2.1392	0.9745	5.5329	645.7	13.4
SU33-21	2564	145	0.06	0.0000	0.2	42.7889	1.7472	0.0499	1.0405	0.1604	2.0494	148.7	2.6
SU45-1	1938	492	0.26	0.0002	0.5	29.3958	0.3141	0.0542	1.0063	0.2374	2.1336	214.7	0.7
SU45-2	3411	264	0.08	0.0041	6.4	24.4791	0.3403	0.1021	1.3962	0.2104	24.3976	242.0	2.2

(continued)

APPENDIX 1. U-Th-Pb DATA FOR ALL SHRIMP ANALYSES OF ZIRCON *(continued)*

Analysis spot	U (ppm)	Th (ppm)	Th/U	$^{204}Pb/^{206}Pb^{*}$	$^{206}Pb^{\dagger}$ (%)	$^{238}U/^{206}Pb^{*}$		$^{207}Pb/^{206}Pb^{*}$		$^{207}Pb/^{235}U^{\#}$		$^{206}Pb/^{238}U$ Age† (Ma)	
SU45-3	3985	290	0.08	0.0000	0.0	28.1146	0.2214	0.0507	0.6822	0.2471	0.8139	225.3	0.5
SU45-4	4083	112	0.03	0.0001	0.2	28.7107	0.2194	0.0523	0.6874	0.2441	1.0380	220.2	0.5
SU45-5	129	84	0.67	0.0023	3.7	25.8993	1.1830	0.0808	3.0923	0.2404	22.5308	235.2	3.1
SU45-6	4809	116	0.02	0.0000	0.1	29.2980	0.1992	0.0509	0.6322	0.2373	0.7670	216.2	0.4
SU45-7	999	642	0.66	0.0000	0.0	29.6796	0.4336	0.0505	1.4089	0.2316	1.6216	213.6	0.9
SU45-8	4117	90	0.02	0.0000	0.1	28.5615	0.2152	0.0511	0.6885	0.2441	0.8147	221.7	0.5
SU45-9	606	362	0.62	0.0000	0.0	29.1516	0.5580	0.0505	1.7997	0.2397	1.8778	217.4	1.2
SU45-10	2688	134	0.05	0.0002	0.4	29.2797	0.2691	0.0538	1.3731	0.2417	2.0753	215.6	0.6
SU45-11	1267	969	0.79	0.0001	0.1	29.5724	0.3852	0.0515	1.2452	0.2321	1.9062	214.1	0.8
SU45-12	3682	60	0.02	0.0000	0.1	29.3036	0.2251	0.0515	0.7279	0.2389	0.8483	216.0	0.5
SU45-13	92	45	0.50	0.0003	0.5	29.1417	1.6212	0.0548	4.5003	0.2379	6.2502	216.3	3.5
SU45-14	197	99	0.52	0.0059	11.7	27.3632	0.9516	0.1437	1.9052	0.2576	33.8395	204.7	4.0
SU45-15	1004	148	0.15	0.0000	0.4	3.1232	0.2829	0.1124	0.5904	4.9646	0.6546	1784.7	5.2
SU45-16	246	145	0.61	–0.0001	0.2	30.5844	0.8592	0.0519	2.7879	0.2381	2.8786	207.0	1.8
SU45-17	150	106	0.73	0.0002	0.4	29.3429	1.1051	0.0537	3.4904	0.2391	4.3890	215.2	2.4
SU45-18	372	230	0.64	0.0001	0.3	29.5458	0.7028	0.0527	2.2698	0.2391	2.5060	214.0	1.5
SU45-19	99	1	0.01	0.0001	0.2	27.5429	1.3629	0.0526	4.2326	0.2535	5.2180	229.4	3.2
SU45-20	351	193	0.57	–0.0002	0.0	29.4515	0.7414	0.0505	2.6482	0.2482	3.5235	215.2	1.6
SU45-21	105	57	0.57	0.0004	0.6	28.7652	1.3487	0.0554	7.7548	0.2381	9.0780	219.0	3.2
SU45-22	370	274	0.77	–0.0001	0.1	28.9095	0.7229	0.0512	2.3122	0.2546	2.3910	219.0	1.6
SU45-23	188	111	0.61	–0.0001	–0.2	29.6738	1.0206	0.0484	2.9539	0.2317	3.0507	214.2	2.2
SU45-24	208	107	0.53	0.0003	0.4	31.7412	1.0520	0.0531	2.9758	0.2077	6.3035	199.2	2.1
SU45-25	343	162	0.49	0.0001	0.2	29.9469	0.8597	0.0516	2.2263	0.2285	2.6617	211.4	1.8
SU45-26	328	163	0.52	0.0000	–0.2	29.5244	0.8498	0.0489	2.2362	0.2316	2.5184	215.1	1.8
SU45-27	1465	455	0.32	0.0036	6.5	28.4295	0.6105	0.1022	1.8652	0.2253	10.4938	208.6	1.6
SU45-28	1339	1192	0.92	0.0000	0.0	28.8101	0.6171	0.0507	1.0554	0.2457	1.3244	219.9	1.3
SU45-29	1027	587	0.59	0.0018	3.4	31.0524	0.6438	0.0770	2.7107	0.2190	10.6003	197.5	1.4
SU45-30	137	79	0.59	0.0008	–0.2	28.8704	1.1424	0.0486	3.3954	0.1747	12.9462	220.0	2.5
SU45-31	625	731	1.21	0.0000	0.1	29.5753	0.7081	0.0508	1.5604	0.2386	1.7556	214.3	1.5
SU45-32	253	142	0.58	–0.0003	0.0	30.1747	0.9268	0.0501	2.5394	0.2481	4.4630	210.2	2.0
SU45-33	349	194	0.57	–0.0001	0.2	29.4484	0.8328	0.0518	2.0986	0.2497	2.2091	214.9	1.8
SU45-34	178	109	0.64	–0.0003	0.0	29.6160	1.0515	0.0500	3.0456	0.2515	3.0429	214.2	2.3
SU45-35	274	264	1.00	0.0023	3.1	29.9381	0.9288	0.0746	4.2793	0.1759	19.2427	205.4	2.1
SU45-36	220	192	0.90	0.0002	0.0	29.6579	0.9518	0.0503	2.6522	0.2161	3.7292	213.8	2.0
SU45-37	115	64	0.57	–0.0002	0.2	28.8775	1.2498	0.0519	3.6830	0.2607	5.2219	219.1	2.8
SU45-38	2026	71	0.04	0.0006	1.1	28.6915	0.6094	0.0589	1.4408	0.2374	4.8091	218.6	1.3
SU45-39	374	193	0.53	0.0001	0.2	29.7667	0.8253	0.0516	2.0542	0.2325	2.3163	212.7	1.8
SU45-40	247	186	0.78	0.0002	0.1	30.0089	0.9442	0.0515	2.5975	0.2241	3.2198	211.0	2.0
SU45-41	107	41	0.39	0.0000	0.3	29.7491	1.2938	0.0532	3.8129	0.2464	4.0264	212.4	2.8
SU45-42	186	104	0.58	0.0001	–0.1	29.7065	1.0256	0.0499	2.9138	0.2245	3.7188	213.6	2.2
SU45-43	1132	60	0.05	0.0001	0.3	28.9065	0.6598	0.0528	1.2801	0.2479	1.8985	218.6	1.4
SU45-44	31	11	0.37	0.0624	91.5	40.8379	2.4156	0.7695	2.8710	N/A	N/A	13.4	10.1
SU45-45	347	194	0.58	0.0000	0.0	29.3477	0.8522	0.0505	2.1898	0.2372	2.3498	216.0	1.8
SU45-46	443	223	0.52	0.0001	0.1	28.9805	0.7901	0.0510	1.9097	0.2334	3.2635	218.6	1.7

Note: 1σ error unless noted otherwise.
*Uncorrected; error given as percentage.
†Corrected for ^{207}Pb.
#Corrected for ^{204}Pb; error given as percentage.

APPENDIX 2. SUMMARY OF ALL HIGH-TEMPERATURE GEOCHRONOMETRY FOR THE SULU AREA

Age (Ma)	Error (±Ma)	Dating method	Type of age	# of analyses	MSWD	Rock type	Reference
U-Pb							
217	9	U-Pb	Intercept	6	N/A	Eclogite	Ames et al., 1996
202	13	U-Pb	Intercept	N/A	N/A	Unknown	Li et al., 1999
223	2	U-Pb IMP	Single-grain	1	N/A	Gneiss	Rumble et al., 2002
220	1	U-Pb IMP	Weighted mean	2	0.6	Garnet peridotite	Rumble et al., 2002
233	2	U-Pb IMP	Single-grain	1	N/A	Garnet peridotite	Rumble et al., 2002
221	12	U-Pb IMP	Probability curve	9	47	Peridotite	Yang et al., 2003
228	29	U-Pb IMP	Intercept	24	1.3	Eclogite	Yang et al., 2003
231	4	U-Pb IMP	Weighted mean	16	1.8	Gneiss	Liu et al., 2004b
208	4	U-Pb IMP	Weighted mean	6	2.2	Gneiss	Liu et al., 2004b
213	5	U-Pb IMP	Weighted mean	6	1.7	Gneiss	Liu et al., 2004b
228	5	U-Pb IMP	Weighted mean	14	1.1	Gneiss	Liu et al., 2004b
247	5	U-Pb IMP	Single-grain	1	N/A	Eclogite	Zheng et al., 2004b
219	8	U-Pb IMP	Single-grain	1	N/A	Eclogite	Zheng et al., 2004b
241	5	U-Pb IMP	Single-grain	1	N/A	Eclogite	Zheng et al., 2004b
217	3	U-Pb IMP	Single-grain	1	N/A	Eclogite	Zheng et al., 2004b
215	6	U-Pb IMP	Single-grain	1	N/A	Eclogite	Zheng et al., 2004b
231	7	U-Pb IMP	Single-grain	1	N/A	Eclogite	Zheng et al., 2004b
229	7	U-Pb IMP	Single-grain	1	N/A	Eclogite	Zheng et al., 2004b
226	7	U-Pb IMP	Single-grain	1	N/A	Eclogite	Zheng et al., 2004b
227	3	U-Pb IMP	Single-grain	1	N/A	Granitic gneiss	Zheng et al., 2004b
258	25	U-Pb IMP	Single-grain	1	N.A	Eclogite	Zheng et al., 2004b
224	14	U-Pb	Intercept	5	4.0	Granitic gneiss	Zheng et al., 2004b
218	16	U-Pb	Intercept	5	6.5	Granitic gneiss	Zheng et al., 2004b
224	27	U-Pb	Intercept	6	7.9	Granitic gneiss	Zheng et al., 2004b
207	1	U-Pb IMP	Weighted mean[#]	11	0.8	Dike	Wallis et al., 2005
222	2	U-Pb IMP	Weighted mean[#]	14	1.3	Dike	Wallis et al., 2005
215	5	U-Pb IMP	Weighted mean	13	N/A	Quartz syenite	Yang et al., 2005
237	8	U-Pb IMP	Weighted mean	30	N/A	Eclogite	Zhao et al., 2005
217	4	U-Pb*	Weighted mean	9	0.4	Granitic gneiss	B.R. Hacker, 2005, pers. comm.
228	2	U-Pb*	Weighted mean	14	0.6	Granitic gneiss	B.R. Hacker, 2005, pers. comm.
224	5	U-Pb*	Weighted mean	3	0.1	Augen gneiss	B.R. Hacker, 2005, pers. comm.
216	2	U-Pb*	Weighted mean	5	0.2	Granitic gneiss	B.R. Hacker, 2005, pers. comm.
202	3	U-Pb*	Weighted mean	6	0.2	Granitic gneiss	B.R. Hacker, 2005, pers. comm.
226	5	U-Pb*	Weighted mean	2	2.3	Granitic gneiss	B.R. Hacker, 2005, pers. comm.
205	3	U-Pb*	Weighted mean	6	N/A	Granitic gneiss	B.R. Hacker, 2005, pers. comm.
219	2	U-Pb*	Weighted mean	7	0.7	Granitic gneiss	B.R. Hacker, 2005, pers. comm.
220	2	U-Pb*	Weighted mean	N/A	0.8	Granitic gneiss	B.R. Hacker, 2005, pers. comm.
226	2	U-Pb*	Weighted mean	N/A	0.6	Granitic gneiss	B.R. Hacker, 2005, pers. comm.
203	3	U-Pb*	Weighted mean	7	N/A	Granitic gneiss	B.R. Hacker, 2005, pers. comm.

(continued)

APPENDIX 2. SUMMARY OF ALL HIGH-TEMPERATURE GEOCHRONOMETRY FOR THE SULU AREA *(continued)*

Age (Ma)	Error (±Ma)	Dating method	Type of age	# of analyses	MSWD	Rock type	Reference
U-Pb							
218	2	U-Pb*	Weighted mean	8	0.0	Granitic gneiss	B.R. Hacker, 2005, pers. comm.
210	8	U-Pb*	Intercept	N/A	1.1	Granitic gneiss	B.R. Hacker, 2005, pers. comm.
210	5	U-Pb IMP	Weighted mean	12	1.7	Granitic gneiss	Liu et al., 2004a
228	5	U-Pb IMP	Weighted mean	17	1.8	Granitic gneiss	Liu et al., 2004a
242	8	U-Pb IMP	Single-grain	1	N/A	Dunite	Zhao et al., this volume.
232	7	U-Pb IMP	Single-grain	1	N/A	Eclogite	Zhao et al., this volume
208	3	U-Pb IMP	Weighted mean	2	0.7	Granitic gneiss	This paper
222	3	U-Pb IMP	Single-grain	1	N/A	Granitic gneiss	This paper
215	2	U-Pb IMP	Single-grain	1	N/A	Granitic gneiss	This paper
232	2	U-Pb IMP	Single-grain	1	N/A	Granitic gneiss	This paper
207	3	U-Pb IMP	Weighted mean	5	0.1	Granitic gneiss	This paper
211	2	U-Pb IMP	Weighted mean	3	0.1	Granitic gneiss	This paper
214	4	U-Pb IMP	Weighted mean	4	0.0	Granitic gneiss	This paper
215	6	U-Pb IMP	Weighted mean	18	0.5	Granitic gneiss	This paper
219	1	U-Pb IMP	Weighted mean	8	0.1	Granitic gneiss	This paper
Sm-Nd							
221	6	Sm-Nd	Isochron - min	2	N/A	Eclogite	Li et al., 1993
209	31	Sm-Nd	Isochron - min	4	N/A	Eclogite	Li et al., 1993
228	6	Sm-Nd	Isochron	N/A	N/A	Unknown	Li et al., 1999
226	4	Sm-Nd	Isochron - min/WR	4	0.9	Eclogite	Li et al., 1999
226	5	Sm-Nd	Isochron - min/WR	4	N/A	Eclogite	Zheng et al., 2002
221	18	Sm-Nd	Isochron - min	2	N/A	Eclogite	Zheng et al., 2002
211	6	Sm-Nd	Isochron - min	2	N/A	Eclogite	Zheng et al., 2002
208	15	Sm-Nd	Isochron - min	2	N/A	Eclogite	Zheng et al., 2002
Rb-Sr							
219	2	Rb-Sr	Isochron - min/WR	3	N/A	Eclogite	Li et al., 1999
224	2	Rb-Sr	Isochron - min/WR	3	N/A	Eclogite	Li et al., 1999

Note: Notation for type of ages: Intercept, lower intercept age on concordia diagram; probability curve, peak on cumulative probability curve; weighted mean, weighted mean age of multiple analyses; single-grain, either age from a single grain or single spot age from ion microprobe analysis; isochron, isochron age for either Sm-Nd or Rb-Sr dating (min, mineral; WR, whole-rock). IMP, ion microprobe analysis; U-Pb, may be age from various methods, including ICP-MS, conventional isotope dilution, etc. N/A, not available in original publication or not applicable. When omitted from original publications and possible from data presented, MSWD was calculated from original data; the number of analyses were calculated or estimated from original data when not explicitly stated in original publications. Errors reported are 1σ. MSWD, mean square of weighted deviates.

*Combination of ion microprobe and ICP-MS U-Pb analyses.

#Weighted mean age calculated for individual analyses reported in Wallis et al. (2005).

APPENDIX 3. SUMMARY OF ALL HIGH-TEMPERATURE GEOCHRONOMETRY FOR THE DABIE–HONG'AN AREA

Age (Ma)	Error (±Ma)	Dating method	Type of age	# of analyses	MSWD	Rock type	Reference
U-Pb/Pb-Pb/Pb-Th							
209	2	U-Pb	Intercept	3	N/A	Eclogite	Ames et al., 1993
212	11	U-Pb	Intercept	4	N/A	Eclogite	Ames et al., 1993
218	2	U-Pb	Intercept	3	N/A	Eclogite	Ames et al., 1996
218	2	U-Pb	Intercept	3	N/A	Eclogite	Ames et al., 1996
214	10	U-Pb	Intercept	3	N/A	Eclogite	Ames et al., 1996
227	22	U-Pb	Intercept	4	N/A	Gneiss	Ames et al., 1996
233	1	U-Pb	Single-grain	N/A	N/A	Sandstone	Bruguier et al., 1997
231	1	U-Pb	Single-grain	N/A	N/A	Sandstone	Bruguier et al., 1997
225	4	U-Pb	Intercept	6	N/A	Eclogite	Rowley et al., 1997
218	2	U-Pb	Intercept	15	N/A	Gneiss	Rowley et al., 1997
225	4	U-Pb IMP	Probability curve	8	N/A	Gneiss	Hacker et al., 1998
236	3	U-Pb IMP	Probability curve	12	N/A	Gneiss	Hacker et al., 1998
224	9	U-Pb	Unknown	N/A	N/A	Unknown	Maruyama et al., 1998, cit. in Hacker and Wang, 1995
236	2	U-Pb	Single-grain	N/A	N/A	Unknown	Li et al., 1999
238	1	U-Pb	Single-grain	N/A	N/A	Unknown	Li et al., 1999
215	5	U-Pb IMP	Weighted mean	8	N/A	Granitic gneiss	Hacker et al., 2000
230	3	U-Pb IMP	Weighted mean	26	0.7	Eclogite	Ayers et al., 2002
236	32	U-Pb IMP	Intercept	11	7.0	Quartzite	Ayers et al., 2002
238	3	U-Pb IMP	Weighted mean	6	0.7	Quartzite	Ayers et al., 2002
223	1	Pb-Th IMP	Intercept	6	N/A	Quartzite	Ayers et al., 2002
209	4	Pb-Th IMP	Isochron	25	0.7	Clinopyroxenite	Ayers et al., 2002
213	3	U-Pb	Intercept	N/A	2.7	Quartzite	Chen et al., 2003
205	12	U-Pb	Intercept	N/A	1.1	Granitic gneiss	Chen et al., 2003
217	4	Pb-Pb	Single-grain	N/A	N/A	Sandstone	Grimmer et al., 2003
226	10	Pb-Pb	Single-grain	N/A	N/A	Sandstone	Grimmer et al., 2003
228	12	U-Pb	Intercept	4	N/A	Granitic gneiss	Zheng et al., 2003
226	8	U-Pb	Intercept	6	N/A	Granitic gneiss	Zheng et al., 2003
222	4	U-Pb IMP	Weighted mean	3	0.1	Eclogite	Li et al., 2004
242	3	U-Pb IMP	Weighted mean	8	2.1	Eclogite	Li et al., 2004
254	30	U-Pb IMP	Intercept	7	2.9	Eclogite	Li et al., 2004
229	12	U-Pb IMP	Weighted mean	8	N/A	Eclogite	Liu et al., 2004c
213	5	U-Pb IMP	Weighted mean	13	N/A	Eclogite	Liu et al., 2004c
229	22	U-Pb IMP	Intercept	5	0.7	Granitic gneiss	Liu et al., 2004c
213	4	U-Pb*	Intercept	5	1.1	Gneiss	Zheng et al., 2004b
222	6	U-Pb*	Intercept	5	0.4	Granitic gneiss	Zheng et al., 2004b
201	14	U-Pb*	Intercept	5	2.9	Granitic gneiss	Zheng et al., 2004b
262	28	U-Pb*	Intercept	5	7.4	Granitic gneiss	Zheng et al., 2004b

(continued)

APPENDIX 3. SUMMARY OF ALL HIGH-TEMPERATURE GEOCHRONOMETRY FOR THE DABIE–HONG'AN AREA *(continued)*

Age (Ma)	Error (±Ma)	Dating method	Type of age	# of analyses	MSWD	Rock type	Reference
Sm-Nd							
229	3	Sm-Nd	Isochron - min/WR	4	N/A	Grt-Bt gneiss	Li et al., 1993
244	11	Sm-Nd	Isochron - min/WR	3	N/A	Eclogite	Li et al., 1993
224	20	Sm-Nd	Isochron - min	3	N/A	Eclogite	Li et al., 1993
221	5	Sm-Nd	Isochron - min	4	N/A	Eclogite	Li et al., 1993
246	8	Sm-Nd	Isochron - min/WR	2	N/A	Eclogite	Okay et al., 1993
246	8	Sm-Nd	Isochron	N/A	N/A	Unknown	Li et al., 1999
226	3	Sm-Nd	Isochron - min/WR	4	0.3	Eclogite	Li et al., 1999
226	3	Sm-Nd	Isochron - min/WR	6	0.1	Gneiss	Li et al., 1999
210	9	Sm-Nd	Isochron - min/WR	3	0.3	Eclogite	Chavagnac and Jahn, 1996
214	7	Sm-Nd	Isochron - min/WR	3	0.4	Eclogite	Chavagnac and Jahn, 1996
211	4	Sm-Nd	Isochron - min/WR	3	0.6	Eclogite	Chavagnac and Jahn, 1996
213	3	Sm-Nd	Isochron - min/WR	2	N/A	Eclogite	Chavagnac and Jahn, 1996
215	5	Sm-Nd	Isochron - min/WR	3	0.5	Eclogite	Chavagnac and Jahn, 1996
218	4	Sm-Nd	Isochron - min	2	N/A	Eclogite	Chavagnac and Jahn, 1996
210	7	Sm-Nd	Isochron - min/WR	3	0.0	Peridotite	Chavagnac and Jahn, 1996
225	7	Sm-Nd	Isochron - min	7	0.7	Garnets	Chavagnac and Jahn, 1996
236	4	Sm-Nd	Isochron - min	4	1.4	Eclogite	Li et al., 2004
Rb-Sr							
240	2	Rb-Sr	Isochron - min/WR	2	N/A	Eclogite	Okay et al., 1993
236	3	Rb-Sr	Isochron - min/WR	2	N/A	Eclogite	Okay et al., 1993
212	5	Rb-Sr	Isochron - min/WR	2	N/A	Eclogite	Chavagnac and Jahn, 1996
223	13	Rb-Sr	Isochron - min/WR	3	7.4	Eclogite	Chavagnac and Jahn, 1996
214	6	Rb-Sr	Isochron - min/WR	3	2.0	Eclogite	Chavagnac and Jahn, 1996
212	19	Rb-Sr	Isochron - min	4	2.5	Phengites	Chavagnac and Jahn, 1996
214	6	Rb-Sr	Isochron - min/WR	4	N/A	Eclogite	Li et al., 1999
223	13	Rb-Sr	Isochron - min/WR	3	N/A	Eclogite	Li et al., 1999
230	7	Rb-Sr	Isochron - min	3	1.9	Eclogite	Li et al., 2004
225	34	Rb-Sr	Isochron - min/WR	3	24	Eclogite	Liu et al., 2004
212	7	Rb-Sr	Isochron - min/WR	5	16	Eclogite	Liu et al., 2004
216	10	Rb-Sr	Isochron - min/WR	4	27	Blueschist	Liu et al., 2004

Note: Notation for type of ages: Intercept, lower or upper intercept age on concordia diagram; Probability curve, peak on probability density curve; Weighted mean, weighted mean age of multiple analyses; Single-grain, either age from a single grain or single spot age from ion microprobe analysis; Isochron, isochron age for either Sm-Nd or Rb-Sr dating (min, mineral; WR, whole-rock). IMP, ion microprobe analysis; U-Pb, may be age from various methods including ICP-MS, conventional isotope dilution, etc. N/A, not available in original publication or not applicable. When omitted from original publications and when possible from data presented, MSWD was calculated from original data; the number of analyses were calculated or estimated from original data when not explicitly stated in original publications. Errors reported are 1σ. MSWD, mean square of weighted deviates.

*Combination of ion microprobe and ICP-MS U-Pb analyses.

#Weighted mean age calculated for individual analyses reported in Wallis et al. (2005).

REFERENCES CITED

Ames, L., Tilton, G.R., and Zhou, G., 1993, Timing of collision of the Sino-Korean and Yangtse cratons: U-Pb zircon dating of coesite-bearing eclogites: Geology, v. 21, p. 339–342, doi: 10.1130/0091-7613(1993)021<0339:TOCOTS>2.3.CO;2.

Ames, L., Zhou, G., and Xiong, B., 1996, Geochronology and isotopic character of ultrahigh-pressure metamorphism with implications for collision of the Sino-Korean and Yangtze cratons, central China: Tectonics, v. 15, p. 472–489, doi: 10.1029/95TC02552.

Ayers, J.C., Dunkle, S., Gao, S., and Miller, C., 2002, Constraints on timing of peak and retrograde metamorphism in the Dabie Shan ultrahigh-pressure metamorphic belt, east-central China, using U-Th-Pb dating of zircon and monazite: Chemical Geology, v. 186, p. 315–331, doi: 10.1016/S0009-2541(02)00008-6.

Black, L.P., Kamo, S.L., Allen, C.M., Davis, D.W., Aleinikoff, J.N., Valley, J.W., Mundil, R., Campbell, I.H., Korsch, R.J., Williams, I.S., and Foudoulis, C., 2004, Improved $^{206}Pb/^{208}U$ microprobe geochronology by the monitoring of a trace-element–related matrix effect: SHRIMP ID-TIMS, ELA-ICP-MS, and oxygen isotope documentation for a series of zircon standards: Chemical geology, v. 205, p. 115–140.

Bruguier, O., Lancelot, J.R., and Malavieille, J., 1997, U-Pb dating on single detrital zircon grains from the Triassic Songpan-Ganze flysch (central China): Provenance and tectonic correlations: Earth and Planetary Science Letters, v. 152, p. 217–231, doi: 10.1016/S0012-821X(97)00138-6.

Chavagnac, V., and Jahn, B.-M., 1996, Coesite-bearing eclogites from the Bixiling Complex, Dabie Mountains, China: Sm-Nd ages, geochemical characteristics and tectonic implications: Chemical Geology, v. 133, p. 29–51, doi: 10.1016/S0009-2541(96)00068-X.

Chen, F., Siebel, W., Guo, J., Cong, B., and Satir, M., 2003, Late Proterozoic magmatism and metamorphism recorded in gneisses from the Dabie high-pressure metamorphic zone, eastern China: Evidence from zircon U-Pb geochronology: Precambrian Research, v. 120, p. 131–148, doi: 10.1016/S0301-9268(02)00162-6.

Cherniak, D.J., and Watson, E.B., 2003, Diffusion in zircon: Reviews in Mineralogy and Geochemistry, v. 53, p. 113–143, doi: 10.2113/0530113.

Cumming, G.L., and Richards, J.R., 1975, Ore lead isotope ratios in a continuously changing earth: Earth and Planetary Science Letters, v. 28, p. 155–171, doi: 10.1016/0012-821X(75)90223-X.

Faure, M., Lin, W., and Le Breton, N., 2001, Where is the North China–South China block boundary in eastern China?: Geology, v. 29, p. 119–122, doi: 10.1130/0091-7613(2001)029<0119:WITNCS>2.0.CO;2.

Faure, M., Lin, W., Monié, P., Le Breton, N., Poussineau, S., Panis, D., and Deloule, E., 2003, Exhumation tectonics of the ultrahigh-pressure metamorphic rocks in the Qinling orogen in east China: New petrological-structural-radiometric insights from the Shandong Peninsula: Tectonics, v. 22, p. 1018, doi: 10.1029/2002TC001450.

Grimmer, J.C., Jonckheere, R., Enkelmann, E., Ratschbacher, L., Hacker, B.R., Blythe, A.E., Wagner, G.A., Wu, Q., Liu, S., and Dong, S., 2002, Late Cretaceous–Cenozoic history of the southern Tan-Lu fault zone: Apatite fission-track and structural constraints from the Dabie Shan (eastern China): Tectonophysics, v. 359, p. 225–253, doi: 10.1016/S0040-1951(02)00513-9.

Grimmer, J.C., Ratschbacher, L., McWilliams, M., Franz, L., Gaitzsch, I., Tichomirowa, M., Hacker, B.R., and Zhang, Y., 2003, When did the ultrahigh-pressure rocks reach the surface? A $^{207}Pb/^{206}Pb$ zircon $^{40}Ar/^{39}Ar$ white mica, Si-in-white mica, single-grain provenance study of Dabie Shan synorogenic foreland sediments: Chemical Geology, v. 197, p. 87–110, doi: 10.1016/S0009-2541(02)00321-2.

Hacker, B.R., and Wang, Q., 1995, Ar/Ar geochronology of ultrahigh-pressure metamorphism in central China: Tectonics, v. 14, p. 994–1006, doi: 10.1029/95TC00932.

Hacker, B.R., Ratschbacher, L., Webb, L.E., Ireland, T., Walker, D., and Dong, S., 1998, U/Pb zircon ages constrain the architecture of the ultrahigh-pressure Qinling-Dabie orogen, China: Earth and Planetary Science Letters, v. 161, p. 215–230, doi: 10.1016/S0012-821X(98)00152-6.

Hacker, B.R., Ratschbacher, L., Webb, L.E., McWilliams, M.O., Ireland, T., Calvert, A., Dong, S., and Wenk, H.-R., 2000, Exhumation of ultrahigh-pressure continental crust in east central China: Late Triassic–Early Jurassic tectonic unroofing: Journal of Geophysical Research, v. 105, p. 13,339–13,364, doi: 10.1029/2000JB900039.

Hacker, B.R., Ratschbacher, L., and Liou, J.G., 2004, Subduction, collision and exhumation in the ultrahigh-pressure Qinling-Dabie orogen, *in* Malpas, J., et al., eds., Aspects of the Tectonic evolution of China: Geological Society of London Special Publication 226, p. 157–175.

Hermann, J., Rubatto, D., Korsakov, A., and Shatsky, V.S., 2001, Multiple zircon growth during fast exhumation of diamondiferous, deeply subducted continental crust (Kokchetav Massif, Kazakhstan): Contributions to Mineralogy and Petrology, v. 141, p. 66–82.

Hoskin, P.W.O., 1998, Minor and trace element analysis of natural zircon ($ZrSiO_4$) by SIMS and laser ablation ICPMS: A consideration and comparison of two broadly competitive techniques: Journal of Trace and Microprobe Techniques, v. 16, p. 301–326.

Leech, M.L., 2001, Arrested orogenic development: Eclogitization, delamination, and tectonic collapse: Earth and Planetary Science Letters, v. 185, p. 149–159, doi: 10.1016/S0012-821X(00)00374-5.

Leech, M.L., Webb, L.E., Yang, T., and Xu, Z., 2003, Microstructural analysis of the ultrahigh-pressure Sulu terrane, eastern China: Eos (Transactions, American Geophysical Union), v. 84, p. F1391.

Leech, M.L., Singh, S., Jain, A.K., Klemperer, S.L., and Manickavasagam, R.M., 2005, The onset of India-Asia continental collision: Early, steep subduction required by the timing of UHP metamorphism in the western Himalaya: Earth and Planetary Science Letters, v. 234, p. 83–97, doi: 10.1016/j.epsl.2005.02.038.

Li, S., Xiao, Y., Liou, D., Chen, Y., Ge, N., Zhang, Z., Sun, S., Cong, B., Zhang, R., Hart, S.R., and Wang, S., 1993, Collision of the North China and Yangtze and formation of coesite-bearing eclogites: Timing and processes: Chemical Geology, v. 109, p. 89–111, doi: 10.1016/0009-2541(93)90063-O.

Li, S., Jagoutz, E., Lo, C.-H., Chen, Y., Li, Q., and Xiao, Y., 1999, Sm/Nd, Rb/Sr, and $^{40}Ar/^{39}Ar$ isotopic systematics of the ultrahigh-pressure metamorphic rocks in the Dabie-Sulu belt, central China: A retrospective view: International Geology Review, v. 41, p. 1114–1124.

Li, X.-P., Zheng, Y.-F., Wu, Y.-B., Chen, F., Gong, B., and Li, Y.-L., 2004, Low-*T* eclogite in the Dabie terrane of China: Petrological and isotopic constraints on fluid activity and radiometric dating: Contributions to Mineralogy and Petrology, v. 148, p. 443–470.

Liou, J.G., Zhang, R.Y., Eide, E.A., Maruyama, S., Wang, X., and Ernst, W.G., 1996, Metamorphism and tectonics of high-*P* and ultrahigh-*P* belts in Dabie-Sulu regions, eastern central China, *in* Yin, A., and Harrison, T.M., eds., The tectonic evolution of Asia: New York, Cambridge University Press, p. 300–343.

Liu, F., Xu, Z., and Xue, H., 2004a, Tracing the protolith, UHP metamorphism, and exhumation ages of orthogneiss from the SW Sulu terrane (eastern China): SHRIMP U-Pb dating of mineral inclusion-bearing zircons: Lithos, v. 78, p. 411–429, doi: 10.1016/j.lithos.2004.08.001.

Liu, F., Xu, Z., Liou, J.G., and Song, B., 2004b, SHRIMP U-Pb ages of ultrahigh-pressure and retrograde metamorphism of gneisses, south-western Sulu terrane, eastern China: Journal of Metamorphic Geology, v. 22, p. 315–326, doi: 10.1111/j.1525-1314.2004.00516.x.

Liu, X., Jahn, B.-M., Liu, D., Dong, S., and Li, S., 2004c, SHRIMP U-Pb zircon dating of metagabbro and eclogites from western Dabieshan (Hong'an block), China, and its tectonic implications: Tectonophysics, v. 394, p. 171–192, doi: 10.1016/j.tecto.2004.08.004.

Ludwig, K.R., 1999, Using Isoplot/Ex, Version 2.01: A geochronological toolkit for Microsoft Excel: Berkeley Geochronology Center Special Publication no. 1a, 47 p.

Ludwig, K.R., 2001, Eliminating mass-fractionation effects on U-Pb isochron ages without doubles-spiking of Pb: Geochimica et Cosmochimica Acta, v. 65, p. 3139–3145, doi: 10.1016/S0016-7037(01)00637-8.

MacDougall, I., and Harrison, T.M., 1988, Geochronology and thermochronology by the $^{40}Ar/^{39}Ar$ method: Oxford Monographs on Geology and Geophysics Volume 9: Oxford, Oxford University Press, 212 p.

McDonough, W.F., and Sun, S.-S., 1995, The composition of the Earth: Chemical Geology, v. 120, p. 223–253, doi: 10.1016/0009-2541(94)00140-4.

Okay, A.I., Sengor, A.M.C., and Satir, M., 1993, Tectonics of an ultrahigh-pressure metamorphic terrane: Dabie Shan, China: Tectonics, v. 12, p. 1320–1334.

Ratschbacher, L., Hacker, B.R., Webb, L.E., McWilliams, M., Ireland, T., Dong, S., Calvert, A., Chateigner, D., and Wenk, H.-R., 2000, Exhumation of the ultrahigh-pressure continental crust in east central China: Cretaceous and Cenozoic unroofing and the Tan-Lu fault: Journal of Geophysical Research, v. 105, p. 13,303–13,338, doi: 10.1029/2000JB900040.

Rowley, D.B., Xue, F., Tucker, R.D., Peng, X., Baker, J., and Davis, A., 1997, Ages of ultrahigh pressure metamorphism and protolith orthogneisses from eastern Dabie Shan: U/Pb zircon geochronology: Earth and Planetary Science Letters, v. 151, p. 191–203, doi: 10.1016/S0012-821X(97)81848-1.

Rubatto, D., 2002, Zircon trace element geochemistry: Partitioning with garnet and the link between U-Pb ages and metamorphism: Chemical Geology, v. 184, p. 123–138, doi: 10.1016/S0009-2541(01)00355-2.

Rubatto, D., and Hermann, J., 2003, Zircon formation during fluid circulation in eclogites (Monviso, western Alps): Implications for Zr and Hf budget in subduction zones: Geochimica et Cosmochimica Acta, v. 67, p. 2173–2187, doi: 10.1016/S0016-7037(02)01321-2.

Rumble, D., Giorgis, D., Ireland, T., Zhang, Z., Xu, H., Yui, T.F., Yang, J., Xu, Z., and Liou, J.G., 2002, Low $\delta^{18}O$ zircons, U-Pb dating, and the age of the Qinglongshan oxygen and hydrogen isotope anomaly near Donghai in Jiangsu Province, China: Geochimica et Cosmochimica Acta, v. 66, p. 2299–2306, doi: 10.1016/S0016-7037(02)00844-X.

Sobolev, N.V., and Shatsky, V.S., 1990, Diamond inclusions in garnets from metamorphic rocks: A new environment for diamond formation: Nature, v. 343, p. 742–746, doi: 10.1038/343742a0.

Tabata, H., Maruyama, S., and Liou, J.G., 1998, Coesite inclusions of zircon from the ultrahigh-pressure Dabie metamorphic terrane, central China: American Geophysical Union, Western Pacific Geophysics Meeting Abstracts, v. 79, p. 152.

Wallis, S., Enami, M., and Banno, S., 1999, The Sulu UHP terrane: A review of the petrology and structural geology: International Geology Review, v. 41, p. 906–920.

Wallis, S., Tsuboi, M., Suzuki, K., Fanning, M., Jiang, L., and Tanaka, T., 2005, Role of partial melting in the evolution of the Sulu (eastern China) ultrahigh-pressure terrane: Geology, v. 33, p. 129–132, doi: 10.1130/G20991.1.

Webb, L.E., Hacker, B.R., Ratschbacher, L., McWilliams, M.O., and Dong, S., 1999, Thermochronologic constraints on deformation and cooling history of high- and ultrahigh-pressure rocks in the Qinling-Dabie orogen, eastern China: Tectonics, v. 18, p. 621–638, doi: 10.1029/1999TC900012.

Webb, L.E., Leech, M.L., Yang, T., and Xu, Z., 2002, Kinematics of structures of the ultrahigh-pressure Sulu terrane, eastern China: Eos (Transactions, American Geophysical Union), v. 83, p. F1245.

Williams, I.S., 1998, U-Th-Pb geochronology by ion microprobe, *in* McKibben, M.A., Shanks, W.C., III, and Ridley, W.I., eds., Applications of microanalytical techniques to understanding mineralizing processes: Reviews in Economic Geology, v. 7, p. 1–35.

Wu, Y.-B., Zheng, Y.-F., and Zhou, J.-B., 2004, Neoproterozoic granitoids in northwest Sulu and its bearing on the North China–South China blocks boundary in east China: Geophysical Research Letters, v. 31, p. L07616, doi: 10.1029/2004GL019785.

Xu, S., Okay, A.I., Shouyuan, J., Sengor, A.M.C., Wen, S., Liu, Y., and Jiang, L., 1992, Diamond from the Dabie Shan metamorphic rocks and its implication for tectonic setting: Science, v. 256, p. 80–82.

Yang, J.-H., Chung, S.-L., Wilde, S.A., Wu, F.-Y., Chu, M.-F., Lo, C.-H., and Fan, H.R., 2005, Petrogenesis of post-orogenic syenites in the Sulu orogenic belt, east China: Geochronological, geochemical and Nd-Sr isotopic evidence: Chemical Geology, v. 214, p. 99–125, doi: 10.1016/j.chemgeo.2004.08.053.

Yang, J.S., Wooden, J.L., Wu, C.L., Liu, F.L., Xu, Z.Q., Shi, R.D., Katayama, I., Liou, J.G., and Maruyama, S., 2003, SHRIMP U-Pb dating of coesite-bearing zircon from the ultra-high-pressure metamorphic rocks, Sulu terrane, east China: Journal of Metamorphic Geology, v. 21, p. 551–560, doi: 10.1046/j.1525-1314.2003.00463.x.

Zhao, R., Liou, J.G., Zhang, R.Y., and Wooden, J.L., 2005, SHRIMP U-Pb dating of zircon from the Xugou UHP eclogite, Sulu terrane, eastern China: International Geology Review, v. 47, p. 805–814.

Zheng, J., Griffin, W.L., O'Reilly, S.Y., Lu, F., Wang, C., Zhang, M., Wang, F., and Li, H., 2004a, 3.6 Ga lower crust in central China: New evidence on the assembly of the North China craton: Geology, v. 32, p. 229–232, doi: 10.1130/G20133.1.

Zheng, Y.-F., Wang, Z.-R., Li, S.-G., and Zhao, Z.-F., 2002, Oxygen isotope equilibrium between eclogite minerals and its constraints on mineral Sm-Nd chronometer: Geochimica et Cosmochimica Acta, v. 66, p. 625–634, doi: 10.1016/S0016-7037(01)00801-8.

Zheng, Y.-F., Gong, B., Zhao, Z.-F., Fu, B., and Li, Y.-L., 2003, Two types of gneisses associated with eclogite at Shuanghe in the Dabie terrane: Carbon isotope, zircon U-Pb dating and oxygen isotope: Lithos, v. 70, p. 321–343, doi: 10.1016/S0024-4937(03)00104-X.

Zheng, Y.-F., Wu, Y.-B., Chen, F.-K., Gong, B., Li, L., and Zhao, Z.-F., 2004b, Zircon U-Pb and oxygen isotope evidence for a large-scale ^{18}O depletion event in igneous rocks during the Neoproterozoic: Geochimica et Cosmochimica Acta, v. 68, p. 4145–4165, doi: 10.1016/j.gca.2004.01.007.

MANUSCRIPT ACCEPTED BY THE SOCIETY 21 SEPTEMBER 2005